Earth and Planetary Science Letters 297 (2010) 18–33

Contents lists available at ScienceDirect

Earth and Planetary Science Letters

journal homepage: www.elsevier.com/locate/epsl

# New late Paleozoic paleopoles from the Donbas Foldbelt (Ukraine): Implications for the Pangea A vs. B controversy

Maud J.M. Meijers [a,b,*], Maartje F. Hamers [a], Douwe J.J. van Hinsbergen [a,c], Douwe G. van der Meer [d], Alexander Kitchka [e], Cor G. Langereis [a], Randell A. Stephenson [f]

[a] Paleomagnetic Laboratory Fort Hoofddijk, Dept. of Earth Sciences, Utrecht University, Budapestlaan 17, 3584 CD Utrecht, The Netherlands
[b] Dept. of Tectonics and Structural Geology, Faculty of Earth and Life Sciences, VU University Amsterdam, De Boelelaan 1085, 1081 HV Amsterdam, The Netherlands
[c] Physics of Geological Processes (PGP), University of Oslo, Physics Building, Sem Sælands vei 24, 0316 Oslo, Norway
[d] Shell International Exploration and Production B.V., Kessler Park 1, 2288 GS Rijswijk, The Netherlands
[e] National Academy of Sciences Ukraine, 55-B Gonchar Street, Kiev 01601, Ukraine
[f] Dept. of Geology and Petroleum Geology, University of Aberdeen, Meston Building, King's College, Aberdeen AB24 3EU, United Kingdom

ARTICLE INFO

*Article history:*
Received 31 December 2009
Received in revised form 1 May 2010
Accepted 20 May 2010
Available online 3 July 2010

Editor: M.L. Delaney

*Keywords:*
paleomagnetism
plate reconstructions
Pangea
Eurasia
inclination shallowing
Paleozoic

ABSTRACT

The Carboniferous to early Permian apparent polar wander (APW) path for Eurasia is not well constrained, because of the paucity of reliable paleomagnetic poles. This is at least partly responsible for the Pangea A vs. B controversy in the early Permian: is the overlap between the northern and southern continents during the early Permian caused by a lack of reliable paleomagnetic data (Pangea A) or must a large displacement along a mega-shear zone be invoked (Pangea B)? Here, we present results from six paleomagnetic sampling sites ranging in age from the early Carboniferous to the early Permian from sedimentary rocks in the Donbas Foldbelt (Ukraine) to improve the Carboniferous–early Permian APW path for Eurasia and to contribute to solving the Pangea A vs. B controversy. Six time intervals were sampled in the Donbas Foldbelt (eastern Ukraine), which was filled with sediments and volcanic units during the late Devonian to Permian syn- and post-rift subsidence phases. We present results from sediments that were corrected for inclination shallowing with the elongation/inclination (*E*/*I*) method. We conclude that there is a general northward movement of the Donbas Foldbelt: the resulting paleolatitudes are slightly but generally significantly higher than expected from existing APW paths. The late Carboniferous to early Permian data provide three new reliable paleopoles for Eurasia. The early Permian pole does not necessarily require a Pangea B reconstruction. It results in higher paleolatitudes for Laurussia in the early Permian and removes the overlap between Gondwana and Pangea. We also reconstructed the position of Laurussia based on Carboniferous Laurentian poles recently corrected for inclination shallowing, which clearly favours a Pangea B configuration. It seems that the Pangea A vs. B debate is as lively as before. The three early Carboniferous paleopoles give reliable paleolatitudes, but declinations significantly deviate from the expected directions. We argue that the southernmost part of the Donbas Foldbelt underwent a counterclockwise rotation, related to Mesozoic compressional events that are recognised in paleostress analyses.



## 1. Introduction

Pangea is the youngest in a series of postulated supercontinents that assembled most of the Earth's continents. The reconstruction of Pangea stems from Wegener's recognition (1915) that the modern Atlantic margins may once have fit together. Subsequently, this assemblage was further constrained by linking similar paleontological and lithostratigraphical paleogeographic domains (Köppen and Wegener, 1924; Du Toit, 1937). The identification of Pangea formed a crucial basis for the concept of plate tectonics, one of the most fundamental discoveries in Earth Sciences. Pangea existed from the late Paleozoic to early Mesozoic, and broke up since the Jurassic, finally leading to the present-day configuration of oceans and continents. For the break-up history an array of geological and geophysical techniques is available, including reconstruction of sea floor spreading through marine magnetic anomalies (Heezen, 1960; Dietz, 1961), hotspot tracks (Richards et al., 1989; Müller et al., 1993; Norton, 2000) and paleomagnetically constrained apparent polar wander (APW) paths (Creer et al., 1954; Besse and Courtillot, 2002; Torsvik et al., 2008a).

The history of assembly as well as the final configuration and subsequent break-up of Pangea is essential to constrain the starting point of our present-day plate tectonic configuration and to define rates and dimensions of plate tectonic motion. The break-up history

* Corresponding author. Paleomagnetic Laboratory Fort Hoofddijk, Dept. of Earth Sciences, Utrecht University, Budapestlaan 17, 3584 CD Utrecht, The Netherlands.
*E-mail address:* meijers@geo.uu.nl (M.J.M. Meijers).

0012-821X/$ – see front matter © 2010 Elsevier B.V. All rights reserved.
doi:10.1016/j.epsl.2010.05.028

can well be constrained through the record of marine magnetic anomalies, but constraining of Pangea's assembly largely relies on APW path reconstructions. Hence, we need more reliable and accurate paleomagnetic poles, because their scarcity leaves room for the ongoing controversy on the position of northern Pangea (Laurussia) with respect to southern Pangea (Gondwana) during the Permo-Carboniferous. In particular, paleomagnetic data provide paleolatitudes and rotations of continents, but no paleolongitude constraints. Depending on the selection of paleomagnetic data, a paleolatitudinal overlap exists between the northern and southern continents in the equatorial realm during the late Carboniferous and Permian, that can be as large as 15° (or ~1650 km). The first recognition of this overlap by Irving (1977) led him to propose a so-called Pangea B configuration (Fig. 1a), in which a shear zone with a mainly longitudinal displacement of ~3500 km during the Permo-Triassic places Gondwana east of Laurussia in the early Permian. On the basis of a new compilation of paleomagnetic data, Morel and Irving (1981) propose a transition from Pangea B to Pangea A to occur mainly in the Permian and Triassic, whereas Torcq et al. (1997) suggest a Triassic transformation. More recently, Muttoni et al. (1996, 2003, 2009) argued for the necessity of a Pangea B type reconstruction on the basis of paleomagnetic data from Adria, as a part of the African plate (Fig. 1a) and propose a transition from Pangea B to Pangea A in the Permian. The Triassic overlap between the northern and southern continents has disappeared, since more paleomagnetic data have become available. Other authors, however, question the necessity for Pangea B, and suggest that the overlap is caused by a lack of sufficient high quality paleomagnetic data (e.g. inclination shallowing due to compaction) (Rochette and Vandamme, 2001; Van der Voo and Torsvik, 2004) or to an octupolar contribution to the Earth's magnetic field (Kent and Smethurst, 1998; Van der Voo and Torsvik, 2001; Torsvik and Cocks, 2004). Most studies (e.g. Van der Voo and Torsvik (2004)) also question the quality of assigned ages.

Numerous authors have attempted solving the Pangea controversy that was identified in paleomagnetic data, by researching independent lines of evidence. Evidence for a shear zone that may have accommodated the Pangea B to Pangea A transformation was first proposed in the late-70s by Arthaud and Matte (1977). Based on their data review on rifts that extend from the Appalachians to the Urals, they conclude that the Pangea transformation occurred in the late Paleozoic. Later studies, by e.g. Schaltegger and Brack (2007) on magmatism related to shearing, seem to confirm the scenario of a Permian Pangea B to A transition. However, a number of rift basins that are possibly associated with Pangea transformation, have been

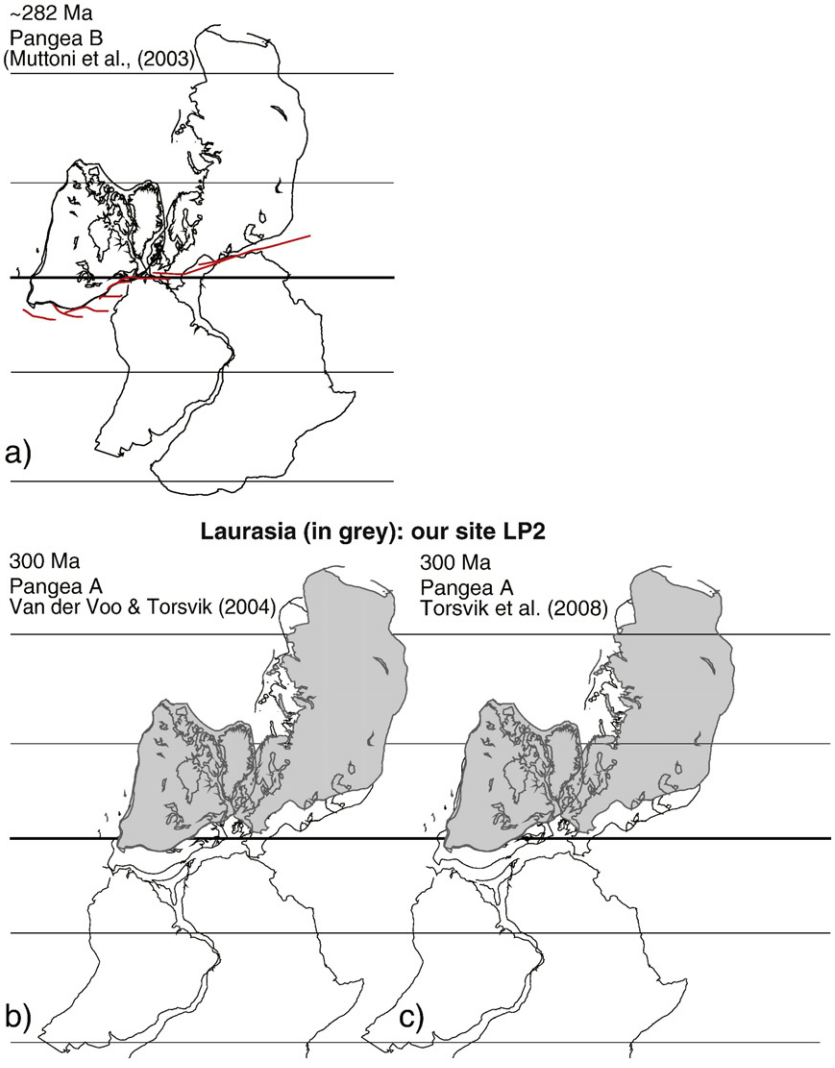


**Fig. 1.** Pangea reconstructions (in white) at a) 282 Ma after Muttoni et al. (2003), where the overlap between the northern and southern continents is removed by introducing a large shear zone (in red). b) in white, reconstruction at 300 Ma following Torsvik and Van der Voo (2002); c) in white, reconstruction at 300 Ma following Torsvik et al. (2008a). b) and c) in grey: Laurussia reconstruction on the basis of our site LP2 (299 Ma). All reconstructions in b) and c) require no overlap between the northern and southern continents. Eurasian (Laurussian) poles are calculated from Laurentian (Eurasian) poles using a Bullard fit (Bullard et al., 1965), with an Euler pole at 88 °N, 27 °E (angle= 38°). Iberia was not included in the reconstructions.

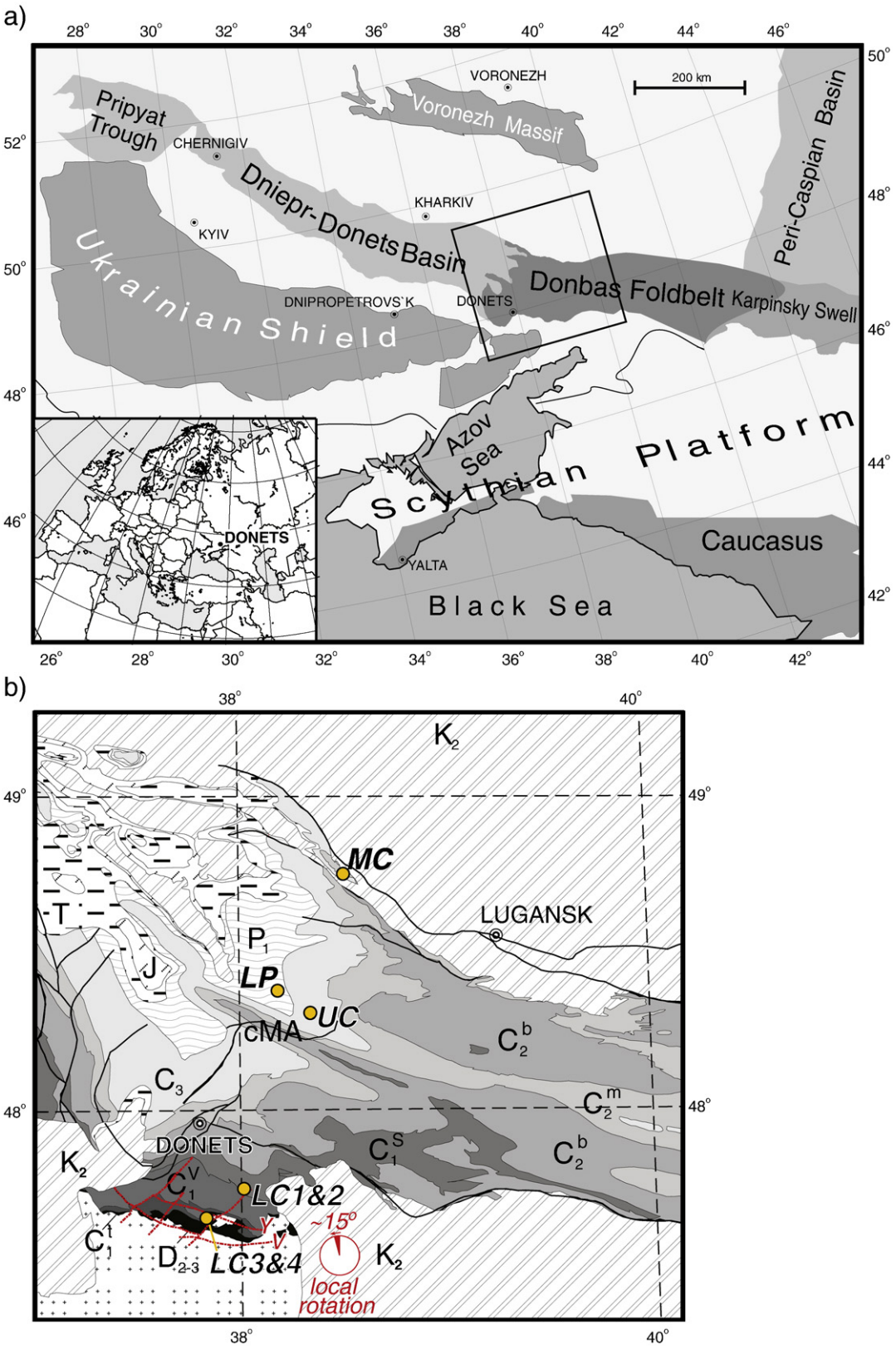


**Fig. 2.** a) Tectonic map of the southern part of the East European Craton, showing the late Devonian Pripyat–Dniepr–Donets rift basin, and the inverted Donbas Foldbelt. Rectangle indicates the location of panel b. b) Cenozoic subcrop map of the Donbas Foldbelt around Donets (modified after Stovba and Stephenson, 1999), indicating the paleomagnetic sampling sites (LC3&4, LC1&2, MC, UC and LP). $D_{2-3}$, Middle Devonian–Upper Devonian; $C_1^t$, Tournaisian; $C_1^v$, Visean; $C_1^s$, Serpukhovian; $C_2^b$, Bashkirian; $C_2^m$, Moscovian; $C_3$, Kasimovian–Gzhelian; $P_1^{as}$, Asselian; $P_1^s$, Sakmarian; T, Triassic; J, Jurassic; $K_2$, Upper Cretaceous; cMA, central Main Anticline. The red dotted lines indicate the major faults that would have possibly caused ~15° counterclockwise rotation of sites LC4, LC3 and LC1_2, as modeled in the study by Saintot et al. (2003b). Y = east–west trending Yujni Fault and V = east–west trending Vassiliev Fault.

**Table 1**
Site, latitude, longitude and assigned ages (with estimated error) from the latest version of the Geological Time Scale, GTS2008 (Ogg et al., 2008) for the sampled sites are given. For reference the ages derived from Menning et al. (2006) and Davydov et al. (2010) are shown. $N_d$ = number of demagnetised specimens, $N$ ($N_{gc}$) = number of total ChRM directions (number of ChRM directions determined with great circles) (McFadden and McElhinny, 1988). $N_{vD}$ = total number of specimens that fall within the Vandamme cut-off angle (Vandamme, 1994), $D$ = declination, $I$ = inclination, $K$ = precision parameter and $\alpha_{95}$ = cone of confidence are all shown for in situ and tilt corrected ChRM directions. For the tilt corrected ChRM directions, the latitude ($\lambda$) and longitude ($\phi$) with corresponding estimate of the precision parameter ($K$) and cone of confidence ($A_{95}$) of the mean virtual geomagnetic pole (VGP) are given and the corresponding paleolatitude ($\lambda$), and declination ($\Delta D_x$) and inclination ($\Delta I_x$) errors are determined from the $A_{95}$ of the poles. The inclination after correction for inclination ($I_{TK}$) error results from 5000 bootstraps of TK03.GAD, with 95% lower and upper bounds ($I_l$, $I_u$), while $I_{EI}$ is the inclination resulting from intersection of the distribution with TK03.GAD (Tauxe and Kent, 2004). palat$_{TK}$ is the corresponding corrected latitude, and $\lambda$, $\phi$, $K$ and $A_{95}$ are as mentioned above for the unflattened datasets. L = Lower and U = Upper. The dip direction/dip of the sampled strata is indicated for each site between brackets after the stage name. In case the dip direction and dip angle vary between parts of the sections, the approximate average is indicated with 'ave'. Rejected sites are indicated in italic font (LP1 and LP2), as well as the results of $E/I$ correction for sites MC1 and MC2 separately, for reasons explained in the text.

| | | | | | | | | In situ | | | | |
|---|---|---|---|---|---|---|---|---|---|---|---|---|
| | | | Age (Ma) | | | | | ChRM directions | | | | |
| Site | Latitude | Longitude | GTS2008 | Menning (2006) | Davydov (2010) | $N_d$ | $N$ ($N_{gc}$) | $N_{vD}$ | $D$ | $I$ | $K$ | $\alpha_{95}$ |
| Svetlodarsk, Kartamysh Fm | | | 299.0 | 296.0 | 298.4 | | | | | | | |
| Asselian (247/11) | | | ±2.0 | ±1.0 | ±1.0 | | | | | | | |
| LP 1 | 48.4031 | 38.2223 | | | | *105* | *97 (56)* | *70* | *221.7* | *−8.5* | | *2.4* |
| LP 1 | 48.4031 | 38.2223 | | | | *105* | *41* | *38* | *224.5* | *−9.3* | | *2.9* |
| LP 2 | 48.4031 | 38.2223 | | | | 67 | 58 (10) | 50 | 214.9 | −20.1 | 87.4 | 2.2 |
| LP 2 | 48.4031 | 38.2223 | | | | 67 | 48 | 40 | 213.9 | −19.7 | 92.3 | 2.4 |
| LP 3 | 48.4031 | 38.2223 | | | | *44* | *43* | *42* | *316.3* | *67.5* | | *2.2* |
| Debaltsevo, ml O-6-1 | | | 303.0 | 301.3 | 303.4 | | | | | | | |
| L. Gzelian (ave 241/18) | | | ±0.5 | ±0.8 | ±0.3 | | | | | | | |
| UC | 48.3493 | 38.3481 | | | | 114 | 110 | 86 | 217.7 | −8.2 | 58.2 | 2.0 |
| Tashkovska, ml K-1 | | | 312.1 | 312.8 | 315.0 | | | | | | | |
| U. Bashkirian (horizontal) | | | ±0.4 | ±0.8 | ±0.0 | | | | | | | |
| MC 1 | 48.7815 | 38.5540 | | | | 95 | 77 | 44 | 224.6 | −16.0 | 19.8 | 5.0 |
| MC 2 | 48.7817 | 38.5540 | | | | 98 | 90 | 42 | 222.5 | −12.7 | 38.2 | 3.6 |
| MC | 48.7817 | 38.5540 | | | | 193 | 167 | 84 | 223.4 | −15.0 | 29.1 | 2.9 |
| Voznosenka, LC1 ml D-3-2, | | | 320.1 | 321.0 | 324.3 | | | | | | | |
| LC2 marker l D-5-1 or D-5-2 | | | ±2.0 | ±1.0 | ±0.6 | | | | | | | |
| Serpukhovian (ave 040/12) | | | | | | | | | | | | |
| LC1_2 | 47.7708 | 38.0389 | | | | 118 | 115 | 91 | 197.4 | −16.4 | 61.8 | 1.9 |
| Styla, Donetsian Horizon | | | 334.5 | 335.3 | 335.5 | | | | | | | |
| Visean (343/09) | | | ±2.5 | ±2.3 | ±2.6 | | | | | | | |
| LC 3 | 47.6760 | 37.8107 | | | | 127 | 102 | 77 | 204.7 | −10.6 | 33.0 | 2.9 |
| Styla, Bazalievian Horizon | | | 353.0 | 355.8 | 358.1 | | | | | | | |
| Tournaisian (014/17) | | | ±1.0 | ±0.8 | ±0.6 | | | | | | | |
| LC 4 | 47.6711 | 37.8040 | | | | 139 | 136 | 117 | 200.2 | −23.9 | 118.1 | 1.5 |

ml = marker limestone.

explained differently by Gutierrez-Alonso et al. (2008). They explain the shear zone in the central part of a Pangea A world and rift basins that are radially positioned in the outer part of Pangea by introducing a novel model of 'self-subduction' of the Pangean plate.

Lines of evidences from climatic reconstructions, based on palynology were investigated by e.g. Angiolini et al. (2007). By coupling palynology, ocean circulation patterns and paleomagnetic data, they reconstruct the early Permian landmasses to a Pangea B configuration. Geophysical data were used by Torsvik et al. (2008b) to develop a hybrid plate motion reference frame that places reconstructed large igneous provinces of the past 300 Myr above the edges of large low shear wave velocity provinces, enabling correlation of surface processes to the deep mantle. In their reconstructions, a Pangea A assemblage of the continents is favoured. Recently, van der Meer et al. (2010) have shown that tomography constrains the paleolongitude of subducted slabs, but this approach unfortunately only has the required resolution until the late Permian (260 Ma), showing a Pangea A configuration at that time. Decades after introduction of the Pangea B configuration, the Pangea controversy remains a matter of debate. The solution could come from enlarging the paleomagnetic database, by supplying well-dated paleomagnetic data from the stable continents.

Only very few Carboniferous paleomagnetic poles exist for Laurussia, which formed the major constituent of northern Pangea. Laurussia included the late Devonian and younger Dniepr–Donets basin in present-day Ukraine (Fig. 2). Here, we present paleomagnetic results of six age intervals from lower Carboniferous to lower Permian sediments in the Donbas Foldbelt, a mildly compressionally deformed segment of the Dniepr–Donets basin, and we discuss the results within the context of the Pangea A vs. B controversy.

## 2. Geological setting

The Donbas Foldbelt is the inverted southeasternmost segment of the NW–SE trending Pripyat–Dniepr–Donets Basin (DDB), which formed since the middle-late Devonian (Stephenson et al., 2006). It is located in the southern part of the East European Craton (EEC) (Fig. 2). The EEC was part of Baltica until the early Paleozoic, after which it amalgamated with Laurentia to form Laurussia. The DDB extends from Belarus to southern Russia, linking with the Karpinsky Swell further to the southeast (Fig. 2a). To the north it is bounded by the (Archean-) Paleoproterozoic Voronezh Massif, to the south by the Ukrainian Shield, also of (Archean-) Paleoproterozoic age. The DDB deepens towards the southeast, with sediments having a maximum thickness of ~2 km in the Pripyat Through in the northwest and ~22 km in the Donbas Foldbelt (Chekunov et al., 1993; Stovba et al., 1996). In middle-late Devonian times pre- and syn-rift sedimentary and volcanic units were deposited on top of the crystalline basement of the EEC followed by the deposition of Carboniferous and Permian post-rift sequences as a result of thermal subsidence in the Permo-Carboniferous (Van Wees et al., 1996). Relatively thin units of Tournaisian and lower Visean carbonates and thick upper Visean to upper Carboniferous successions of dominantly paralic clastic sediments were deposited unconformably on top of the basement and the Devonian sediments (Stovba et al., 1996). Permian sediments are scarce in the Donbas Foldbelt, and confined to the north of the basin

| Tilt corrected | | | | | | | | | | | | | | | | | | | | |
|---|---|---|---|---|---|---|---|---|---|---|---|---|---|---|---|---|---|---|---|---|
| ChRM directions | | | | | | | | VGPs | | | | TK03.GAD | | | | | TK03.GAD–VGPs | | | |
| $N_{vD}$ | $D$ | $\Delta D_x$ | $I$ | $\Delta I_x$ | $\lambda$ | $K$ | $\alpha_{95}$ | $\lambda$ | $\phi$ | $K$ | $A_{95}$ | $I_{EI}$ | $I_I$ | $I_{TK}$ | $I_u$ | palat$_{TK}$ | $\lambda$ | $\phi$ | $K$ | $A_{95}$ |
| *70* | *220.5* | *2.2* | ***−18.7*** | *4.1* | | | *2.4* | | | *61.0* | *2.2* | | | | | | | | | |
| *38* | *223.3* | *2.6* | ***−19.7*** | *4.8* | | | *2.9* | | | *78.9* | *2.6* | | | | | | | | | |
| 50 | 212.0 | 1.8 | **−29.5** | 2.8 | **15.8** | 87.4 | 2.2 | 48.2 | 168.3 | 87.4 | 1.7 | | | | | | | | | |
| 40 | 211.0 | 1.8 | **−29.0** | 2.8 | **15.5** | 92.3 | 2.4 | 48.4 | 169.8 | 178.8 | 1.7 | | | | | | | | | |
| *42* | *295.8* | *3.0* | ***61.6*** | *2.5* | | | *2.2* | | | *56.4* | *3.0* | | | | | | | | | |
| 86 | 215.5 | 1.7 | **−24.3** | 3.0 | **12.7** | 58.4 | 2.0 | 43.8 | 166.5 | 80.9 | 1.7 | −33.5 | −27.7 | **−33.0** | −39.7 | **18.0** | 48.2 | 162.3 | 69.3 | 1.8 |
| 44 | 224.6 | 3.9 | **−16.0** | 7.4 | **8.2** | 19.8 | 5.0 | 34.8 | 160.7 | 31.9 | 3.9 | *−21.3* | *−14.7* | ***−22.0*** | *−31.2* | *11.4* | | | | |
| 42 | 222.5 | 3.0 | **−12.7** | 5.8 | **6.4** | 38.2 | 3.6 | 34.5 | 164.0 | 56.0 | 3.0 | *−19.5* | *−12.6* | ***−17.3*** | *−28.2* | *8.9* | | | | |
| 84 | 223.4 | 2.3 | **−15.0** | 4.4 | **7.6** | 29.1 | 2.9 | 35.0 | 162.3 | 44.5 | 2.3 | −22.0 | −16.8 | **−22.4** | −28.8 | **11.6** | 38.4 | 159.5 | 35.4 | 2.6 |
| 89 | 197.2 | 1.3 | **−10.3** | 2.5 | **5.2** | 105.9 | 1.5 | 44.9 | −166.6 | 142.3 | 1.3 | −20.8 | −15.5 | **−20.5** | −25.7 | **10.6** | 50.2 | −169.0 | 104.0 | 1.5 |
| 76 | 203.6 | 2.1 | **−3.9** | 4.2 | **2.0** | 34.1 | 2.8 | 39.9 | −173.7 | 62.5 | 2.1 | −5.2 | −2.1 | **−5.9** | −9.7 | **3.0** | 40.8 | −174.1 | 45.0 | 2.5 |
| 118 | 199.9 | 1.1 | **−7.4** | 2.2 | **3.7** | 76.2 | 1.5 | 42.8 | −169.8 | 131.3 | 1.1 | −10.0 | −7.4 | **−9.7** | −13.1 | **4.9** | 43.9 | −170.3 | 111.1 | 1.2 |

(Stovba and Stephenson, 1999). Reactivation of the rift occurred during the end of the late Visean and during latest Carboniferous–earliest Permian times (Stovba et al., 2003; Stephenson et al., 2006).

After the Paleozoic, the Donbas basin was deformed by large-scale WNW to ESE striking faults and folds, of which the central Main Anticline is the most dominant feature (Fig. 2b). The origin of these folds and faults was formerly ascribed to a compressional period in the Permian, but recently (Stephenson et al., 2006) argued that subtle deformation of Permian age was caused by salt tectonics in a transtensional setting. Saintot et al. (2003a) and Stovba and Stephenson (1999) propose two post-Paleozoic compressional phases that caused basin inversion: a latest Triassic–earliest Jurassic Cimmerian phase and a latest Cretaceous–earliest Paleogene Alpine phase, leading to erosion and exposure of the basin's stratigraphy.

## 3. Paleomagnetic sampling, methods and results

### 3.1. Sampling procedure and age of sampled formations

For the purpose of constructing a late Paleozoic APW path from the Donbas Foldbelt, we collected 724 samples from eleven sites at five localities, covering six time intervals, north and south of the city of Donets (Table 1, Fig 2b). The Carboniferous lithostratigraphy of the Donbas Foldbelt is in the former Soviet Union traditionally subdivided into suites (Popov, 1965). These suites have been correlated to the regional stratigraphic substages and to the global stratigraphic scales; for the most recent overview and compilation we refer to Menning et al. (2006). Recently, Davydov et al. (2010) have provided new results on U–Pb ages and Milankovitsch cyclicity in the Donets Basin, and calibrated the regional time scale to the global time scale, essentially confirming the earlier correlation of Menning et al. (2006). We indicated the ages of the sampled marker limestones and horizons, according to Menning et al. (2006) and Davydov et al. (2010) in Table 1. To allow comparison of our data to the APW paths, we correlated the regional substages to the latest version of the Geologic Time Scale, GTS2008 (Ogg et al., 2008) Those ages are indicated in Table 1 and Fig. 3.

The oldest sampled rocks have a Tournaisian (early Carboniferous) age, the sites with the youngest rocks represent the Gzhelian (latest Carboniferous) to Asselian (early Permian). All Carboniferous samples were collected from limestones, except for one upper Carboniferous site (MC2) that was drilled in claystones. The upper Carboniferous to lower Permian sites (LP1, LP2 and LP3) were sampled in sandy red beds. We sampled the rocks by drilling standard paleomagnetic cores, using a gasoline powered motor drill or an electric drill with generator. Most sites consist of 50–100 cores, the majority of which were long enough to provide two or more specimens. In total, 749 cores were drilled. Sample orientations were measured with a magnetic compass; we corrected the sample orientations and measured bedding planes for the present-day 007°E declination. The samples we collected were mostly large enough to provide two or more specimens, and 907 specimens were demagnetised.

### 3.2. Methods

The anisotropy of magnetic susceptibility (AMS) was measured (Fig. 4) to determine the magnetic fabric of the sediments and to

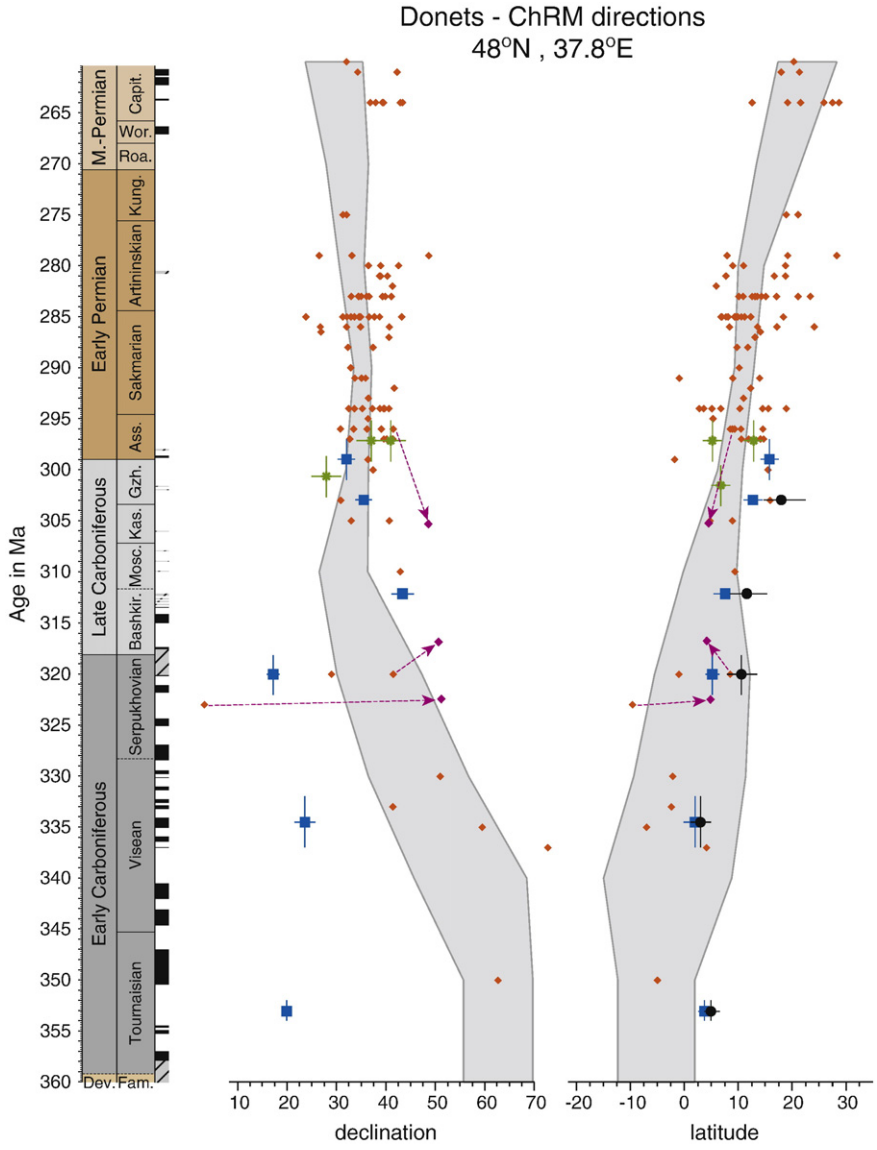


**Fig. 3.** Paleomagnetic directions, correlated to the GTS2008 (Ogg et al., 2008), see Section 3.1 for explanation. Vertical bars denote age errors. Blue closed squares indicate the mean formation directions (declination, latitude) and their errors (blue horizontal bars, $\Delta D_x$, $\Delta\lambda$ (calculated from $\Delta I_x$)) from the present study (Table 1). Black closed circles in the right panel indicate paleolatitude resulting from inclination correction with the TK03.GAD model (Tauxe and Kent, 2004), and horizontal bars shows the 95% bootstrap error range. Green star indicates data points from Iosifidi et al. (2010) (one late Carboniferous and two Permian data points). Grey shaded area shows the $\Delta D_x$, $\Delta\lambda$ error envelope of the Eurasian APW path from Torsvik et al. (2008a) for 310–260 Ma and the Laurussia polepath from Torsvik and Cocks (2005) for 360–320 Ma, calculated for the city of Donets (48°N, 37.8°E). Red diamonds are the raw data entries from Eurasia and North America used to construct these APW paths. Purple arrows and diamonds show the effect of correction for inclination error and improvement of dating of North American poles by Kodama (2009) and Bilardello and Kodama (2010) on the declination/latitude calculations for the Donbas. Dev. = Devonian, Fam. = Famennian, Bashkir. = Bashkirian, Mosc. = Moscovian, Kas. = Kasimovian, Gzh. = Gzhelian, Ass. = Asselian, Kung. = Kungurian, Roa. = Roadian, Wor. = Wordian, Capit. = Capitanian, and GPTS = geomagnetic polarity time scale.

assess whether they have a mainly sedimentary fabric or a tectonic fabric that may be indicative of the amount of strain that the rocks underwent since their deformation (Hrouda, 1982). During deformation, the maximum axis of the AMS tensor ($k_{max}$) will gradually align with the direction of maximum extension and become perpendicular to the direction of maximum compression. For calculations Jelinek (Jelinek, 1981, 1984) statistics were used.

Thermomagnetic runs to determine magnetic carriers were carried out in air (Fig. 5), using a modified horizontal translation type Curie balance, with a sensitivity of $\sim 5\times10^{-9}$ Am$^2$ (Mullender et al., 1993). Approximately 30–65 mg of powdered rock samples was put into a quartz glass sample holder and was held in place by quartz wool. Heating and cooling rates were 10 °C/min. Temperatures were increased to a maximum of 700 °C.

The samples were demagnetised using alternating field (AF) and thermal (TH) progressive stepwise demagnetisation. Samples were thermally demagnetised in a magnetically shielded oven, with steps of 10 °C–100 °C up to a maximum of 645 °C. The AF demagnetisation was carried out with increments of 3–20 mT, up to a maximum of 80 or 100 mT. The natural remanent magnetisation (NRM) of all samples was measured on a 2G Enterprises horizontal 2G DC SQUID cryogenic magnetometer (noise level $3\times10^{-12}$ Am$^2$). For AF demagnetisation, we used an in-house developed robot assisted and fully automated 2G DC SQUID cryogenic magnetometer.

Demagnetisation diagrams of the NRM were plotted as orthogonal vector diagrams (Zijderveld, 1967) (Fig. 6). To determine characteristic remanent magnetisation (ChRM) directions, results from generally five to eight successive temperature or AF steps were analysed by principal component analysis (Kirschvink, 1980). In several cases, samples with a direction that deviated from the general NRM behaviour were analysed using the great-circle approach (McFadden and McElhinny, 1988) (Fig. 6c). This method was developed to identify

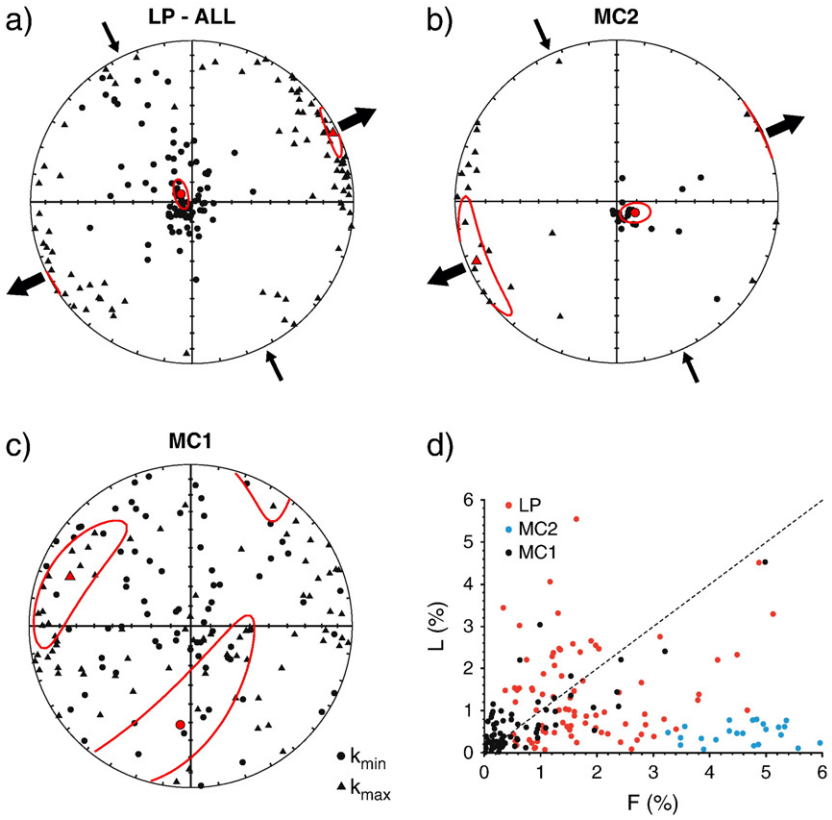


**Fig. 4.** a), b) and c) Equal area projections of the AMS (anisotropy of the magnetic susceptibility) for characteristic sites in tilt corrected coordinates. Grey, large symbols indicate the mean of the individual directions and their error ellipses (Jelinek, 1981). Thick (thin) arrows represent inferred extension (compression) directions. d) Flinn diagram for AMS measurements of sites LP, MC2 and MC1. $L$ (%)>$F$ (%) denotes a prolate magnetic fabric, $F$ (%)>$L$ (%) an oblate fabric.

the direction on the great circle that lies closest to the average direction obtained from well-determined NRM directions. Samples yielding maximum angular deviation (MAD) >15° were rejected from further analysis. A total of 907 specimens was demagnetised, from 749 samples. Of these, the results of 503 demagnetisations were used to calculate the final paleomagnetic poles (Table 1).

Fisher statistics (Fisher, 1953) were used to calculate site-means and virtual geomagnetic pole (VGP) means. Because scatter of paleomagnetic directions induced by secular variation of the Earth's magnetic field is circular at the poles, but gradually becomes more ellipsoid towards the equator (Tauxe and Kent, 2004), we calculated the VGPs from all directions. Successively, a variable cut-off (Vandamme, 1994) was applied and the error in declination ($\Delta D_x$) and the error in inclination ($\Delta I_x$) of the site were calculated following Butler (1992).

To determine whether two distributions have a common true mean direction (ctmd), we used the reversal test developed by McFadden and McElhinny (1990) and their classifications (A, B, C, indeterminate). The classifications are based on the critical angle $\gamma_c$ and the angle $\gamma$ between the means. Because we use their test with simulation, the test is equivalent to using the $V_w$ statistical parameter of Watson (1983).

To correct for a possible shallowing of inclination in sediments caused by compaction during burial, we used the elongation/inclination ($E/I$) method (Tauxe and Kent, 2004; Tauxe et al., 2008). A large number of individual directions are required to apply the model successfully (preferably $N$>100). Since the number of individual directions from our sites varies from 50 to 118, we will discuss the validity of using this correction per locality.

### 3.3. Paleomagnetic results

The AMS measurements of sites LP and MC2 (Fig. 4a and b) show an alignment of the $k_{max}$ axis, which may have been caused by an ENE–WSW extensional or a NNW–SSE compressional episode, or by transport current directions during the time of deposition. The AMS measurements of all other sites revealed random directions, with very large error ellipses (e.g. Fig. 4c) (Jelinek, 1981, 1984), and cannot be interpreted in terms of an AMS fabric. Flinn diagrams of the AMS measurements (Fig. 4d) show that MC2 is strongly oblate, likely because of more compaction of these clays than of the limestones, while the reds of site LP show a mixture of oblate and prolate fabrics. The dominant prolate fabric of site MC1 has little meaning of a random AMS fabric (Fig. 4c), likely caused by the low intensities of the limestones and a relatively large diamagnetic contribution.

From all sites, test sets of samples were demagnetised both thermally and using AF demagnetisation, to allow comparison of both techniques (Fig. 6), similar to the procedures in Gong et al. (2008b). This implies that all AF demagnetised samples were first heated to 150 °C to remove possible stress in magnetite grains caused by surface oxidation at low temperatures (Van Velzen and Zijderveld, 1995), except for the clays of site MC2. Our tests showed that the limestones of site UC should be pre-heated to higher temperatures, until 250 °C or 300 °C before AF demagnetisation. In general, this pre-heating technique appeared very successful, since the overprint direction could already be removed at significantly lower AF fields. The lower Permian (LP) sites were not demagnetised using AF treatment, since

**Fig. 5.** a)–j) Thermomagnetic curves measured on a Curie balance (Mullender et al., 1993) for characteristic samples of each site. Arrows indicate heating (red) and cooling (blue) curves.

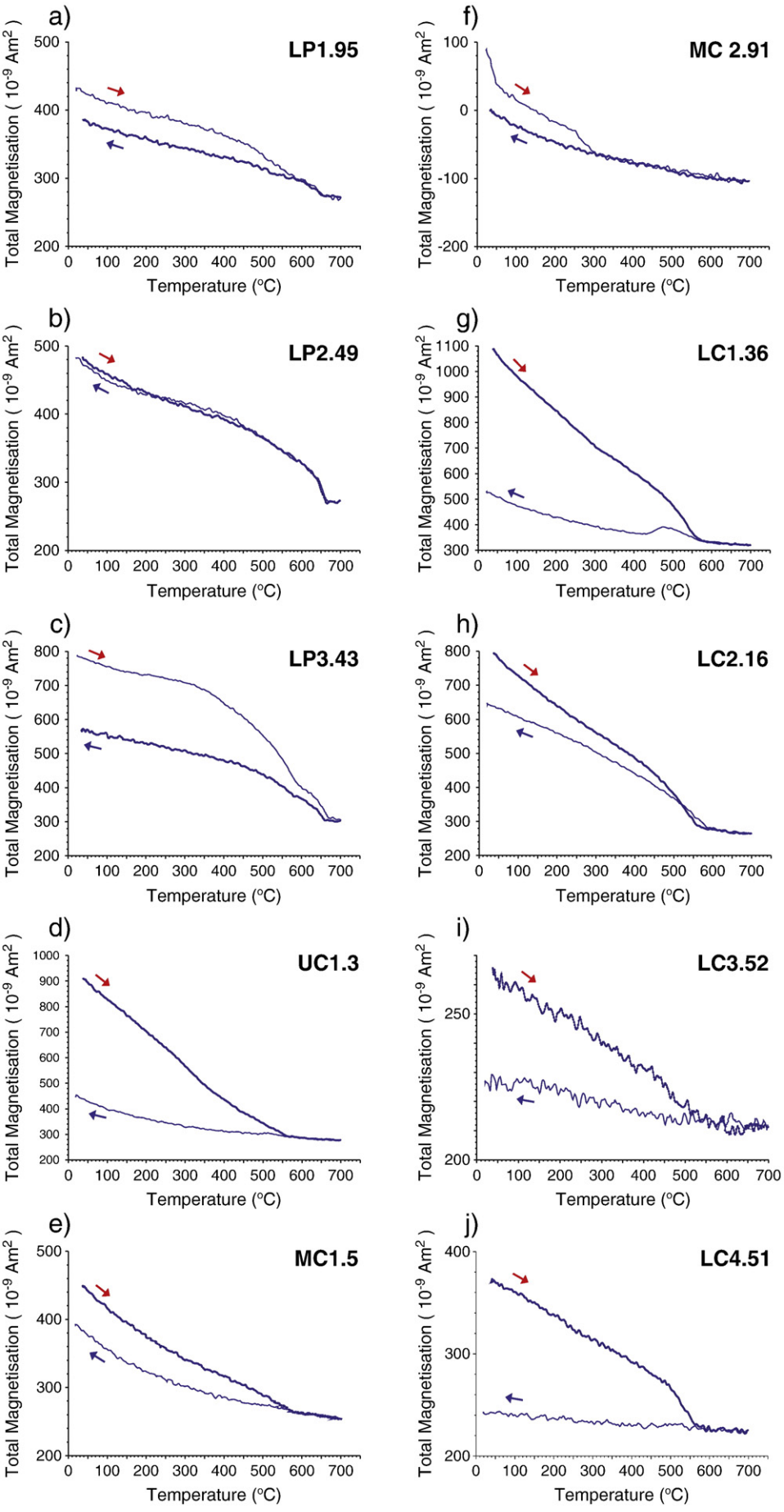
a)
LP1.95
b)
LP2.49
c)
LP3.43
d)
UC1.3
e)
MC1.5
f)
MC 2.91
g)
LC1.36
h)
LC2.16
i)
LC3.52
j)
LC4.51
Total Magnetisation ( 10-9 Am2 )
Temperature (°C)

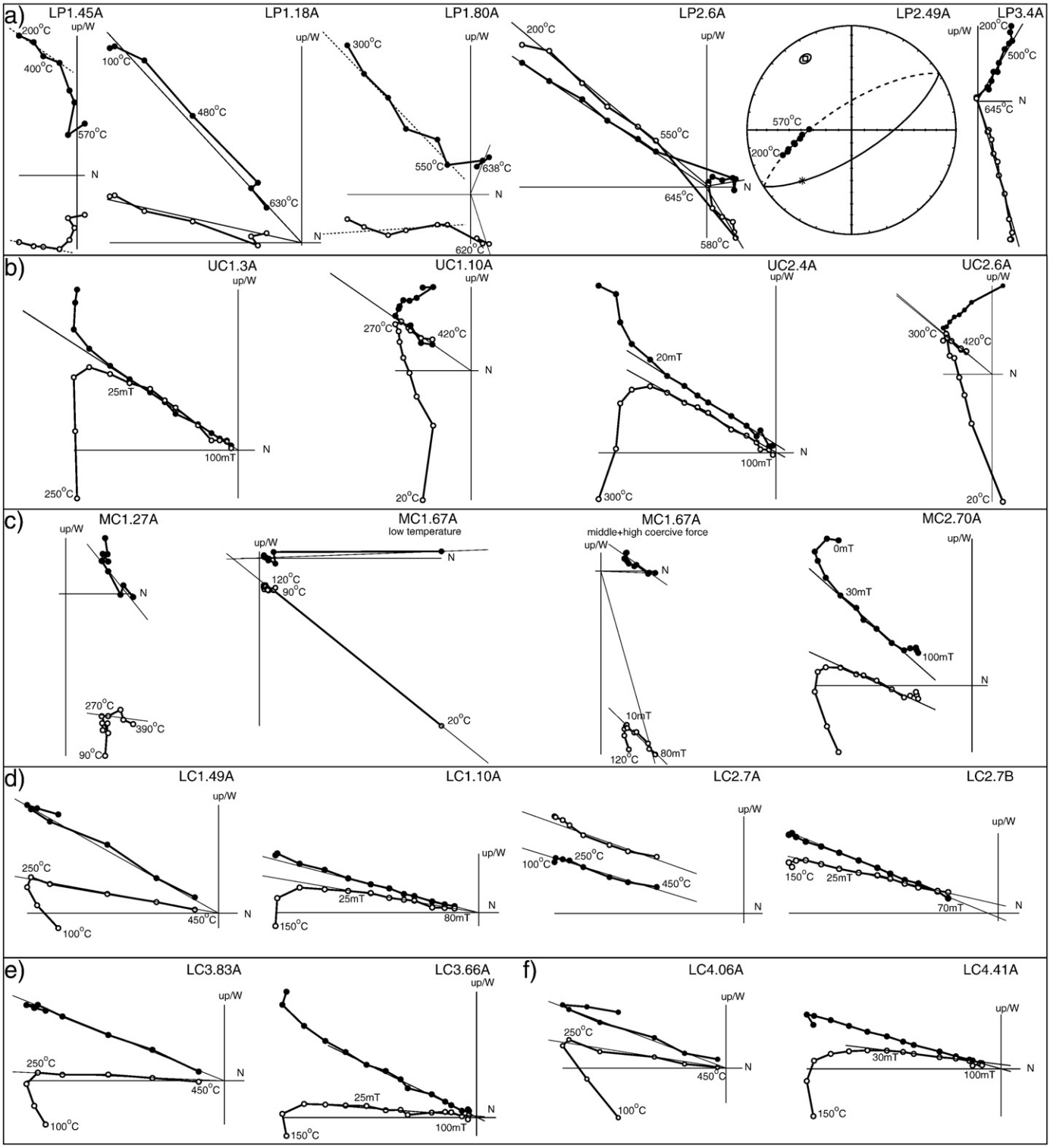


**Fig. 6.** Orthogonal vector diagrams (Zijderveld, 1967), showing characteristic demagnetisation diagrams for all sampled sites in tilt corrected coordinates. Closed (open) circles indicate the projection on the horizontal (vertical) plane. Dashed lines in a) (LP1.45A and LP1.80A) indicate the steps that were used for great-circle analysis (McFadden and McElhinny, 1988). In Fig. 5a), c) and d), the remaining magnetisation after thermal or AF demagnetisation can be seen (LP1.80A, MC1.27A, MC1.67A and LC2.7A). These components are also displayed in Fig. 7b)–d). The demagnetisation diagram of specimen MC1.67A is shown twice, to display the three distinct directions: the low temperature component that resembles the present-day GAD direction, the medium coercive force component (interpreted as the primary ChRM) and the remaining high coercive force component after full AF demagnetisation, that is close to the present-day GAD direction. An equal area plot of a demagnetisation diagram that was interpreted using great-circle analysis is shown in a) (LP2.49A): dashed (solid) line denotes projection on lower (upper) hemisphere.

the maximum applicable alternating field (100 mT) was not high enough to fully demagnetise the hematite-bearing samples.

From most sites, a low temperature/low coercive force component could be isolated, that is indistinguishable from the GAD field at the present latitude (Fig. 7a) and is therefore a recent overprint. Only in site LP, we did not observe this low temperature GAD field, because nearly all samples were pre-heated until 200 °C.

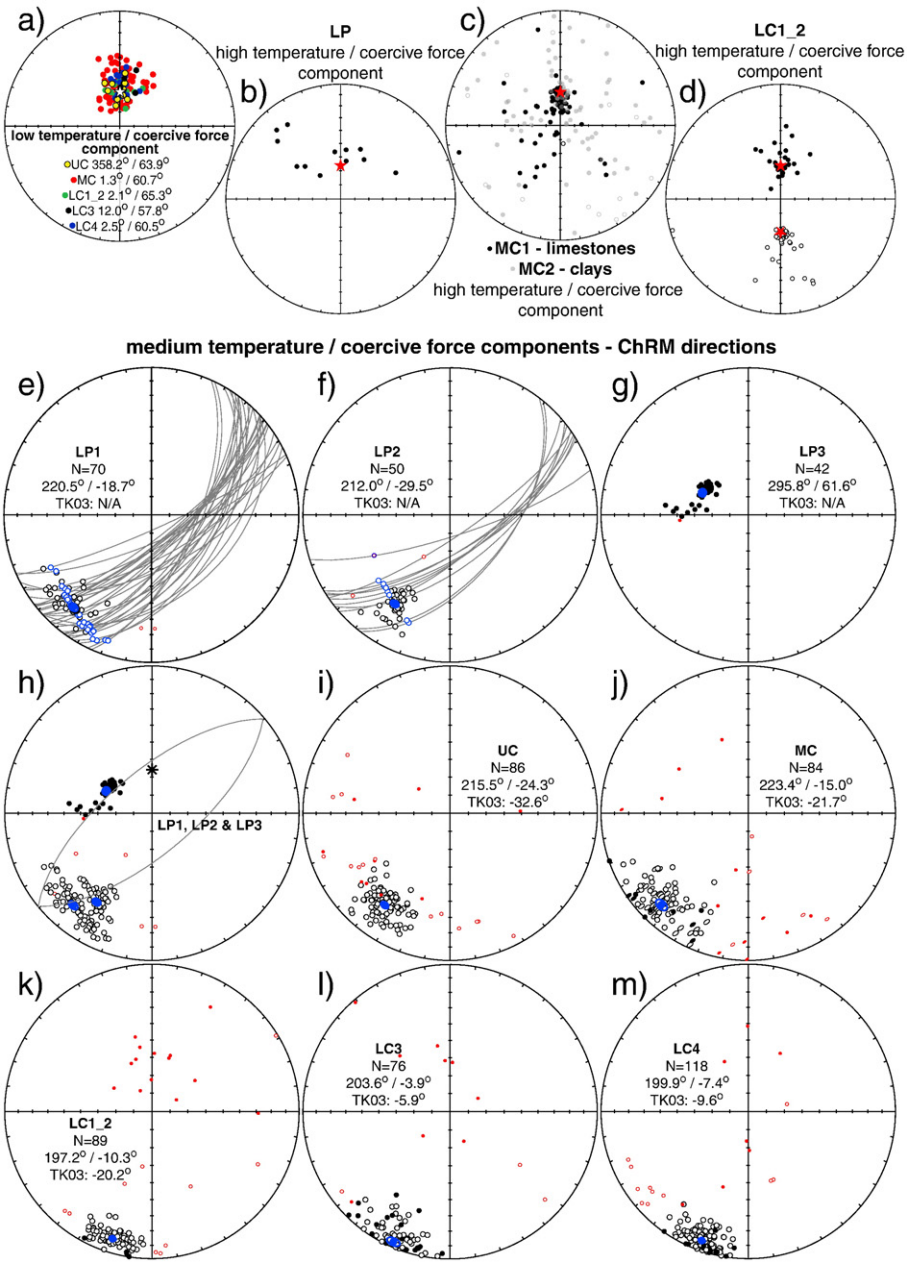


**Fig. 7.** a)–d) in situ: a) low temperature/low coercive force component of sites UC, MC, LC1_2, LC3 and LC4. See Section 3.3.2 for explanation. Colour coding according to the colours in the figure. White star indicates the GAD field direction at the current latitude. b)–d) High temperature high/coercive force component. We interpreted the remaining magnetisation after AF or thermal demagnetisation towards the origin. The remaining magnetisation clearly represents a recent field direction (red star denotes present-day GAD field). In the clays of site MC2 the directions are more random, see text for explanation. e)–m) tilt corrected: equal area projections of the ChRM directions of all sites (Table 1). Open and closed circles indicate the individual directions. Blue symbols indicate respectively the mean directions and their cone of confidence ($\alpha_{95}$; not always visible). Red (small) circles indicate the individual directions rejected by the Vandamme cut-off angle (Vandamme, 1994). Solid (open) symbols are lower (upper) hemisphere projections. Number of individual directions after applying the Vandamme cut-off ($N$), declination, inclination and inclination after $E/I$ correction are indicated. In e) and f) black lines indicate the great circles that were used to calculate the best fitting ChRM directions (McFadden and McElhinny, 1988), the corresponding directions are indicated in blue. h) Equal area projection of all Permian (Asselian) sites, with their individual site-mean direction. Black star indicates the present-day geo-axial dipole (GAD) position in the Donbas Foldbelt. Great circle (best fitting) through LP1, LP2, LP3 and the GAD indicates the transition from an Asselian direction in LP2 increasingly toward the present-day GAD overprint directions of LP1 and LP3. j) Equal area projections of the ChRM directions of site MC. Individual directions of MC1 (limestones) are represented by circles, and individual directions of MC2 (claystones) are represented by ovals.

In samples from sites LP, we observed a high temperature component between 580 °C and ~640 °C (Fig. 6a, LP1.18A and LP1.80A). This component, although not very often observed, yields a direction that seems to be resulting from a present-day overprint (Fig. 7b). Samples from sites MC1, MC2 and LC1_2 could in ~40% of the samples not be demagnetised to the origin using AF demagnetisation techniques (cf. Fig. 6c and d). Using thermal demagnetisation techniques, we could not isolate this component (e.g. Fig. 6c and d), because of magnetite generation and random natural remanent magnetisation (NRM) behaviour at temperatures above ~400–450 °C. This indicates that there is a remaining hematite component in the samples. When interpreting this remaining component towards the origin, it is indistinguishable from the GAD field for sites MC1 and LC1_2 (Fig. 7c and d). This component has both normal and reversed polarities in site LC1_2, which indicates that it results from a recent overprint that at least in part predates the Brunhes Chron.

In site MC, this component is more disperse (Fig. 7c), particularly in the clays of MC2, but most directions of the limestones of MC1 are close

to the present-day GAD field. This may indicate that the remagnetisation is of chemical origin, possibly resulting from circulating fluids. In this case, clays would function as an aquitard, being more resistant to fluid circulation than the directly underlying limestones (MC1). A similar process has then likely occurred in the limestones of sites LC1_2. The fluids likely derive from burial and pressure dissolution of calcite, with the lithological effect that limestones are more prone to remagnetisation than marls. It is less likely that externally derived fluids have played an important role (Gong et al., 2008a).

### 3.3.1. Tournaisian

Site LC4 was sampled in lower Carboniferous (Tournaisian B) limestones. The stratigraphic thickness of the sampled interval is 23 m. It comprises 139 demagnetised specimens, from which 8 were demagnetised thermally and 131 using combined thermal and AF demagnetisation (Fig. 6f). Initial intensities range from ~50 to 500 μA/m. Curie temperatures are 570 °C–580 °C (Fig. 5j), indicating that the magnetic carrier in the samples is magnetite. After application of our criteria, the ChRM corrected for bedding tilt for this site ($N=118$) is $D=199.9$, $I=-7.4$ (Table 1, Fig. 7m). Correction for inclination shallowing results in slight and is not significant, within the 95% bootstrap errors, changing the inclination to $I=-9.7$ (Fig. 8; Table 1).

### 3.3.2. Visean

The samples of site LC3 were taken from lower Carboniferous (Visean) limestones and were sampled in 16.5 m of stratigraphy. Site LC3 consists of 127 demagnetised specimens, from which five were demagnetised thermally and the remaining specimens by combined thermal and AF demagnetisation (Fig. 6e). Initial intensities range from ~50 to 500 μA/m. Curie temperatures are between 520 °C and 580 °C (Fig. 5i), indicating that the main magnetic carrier is (Ti-poor) magnetite. For many specimens, we could not reliably determine the ChRM, caused by very low intensities between 550 °C and 600 °C. The resulting mean ChRM ($N=76$), corrected for bedding tilt is $D=203.6$ and $I=-3.9$ (Table 1, Fig. 7l). Correction for inclination shallowing yields again a not significant correction to $I=-5.9$.

### 3.3.3. Serphukovian

The fossiliferous and locally sandy limestones of the combined sites LC1_2 are early Carboniferous (late Serpukhovian) in age. The stratigraphic thickness of the sampled interval is several meters thick. Site LC1_2 consists of 118 demagnetised specimens, of which 12 specimens were demagnetised thermally, 106 using combined thermal and AF demagnetisation (Fig. 6d). Initial intensities range from ~1 to 5 mA/m. Curie temperatures are 560 °C–570 °C (Fig. 5g and h). In some samples, an inflection around 300 °C may indicate an inversion of maghemite (Fig. 5g). The resulting ChRM ($N=89$) after correction for bedding tilt is $D=197.2$, $I=-10.3$ (Fig. 7k). The correction for inclination shallowing is statistically significant ($I=-20.5$), although the number of samples is quite low ($N<100$).

### 3.3.4. Bashkirian

The samples of the combined sites MC1 and MC2 (sampled stratigraphy interval ~1 and 1.5 m, respectively) were taken from upper Carboniferous (Bashkirian) limestones and claystones. Locality MC provided 193 demagnetised specimens; 17 specimens were fully demagnetised thermally and 176 using AF demagnetisation (the clays) or combined thermal and AF demagnetisation (the limestones) (Fig. 6c). Initial intensities of the limestone specimens (MC1) range

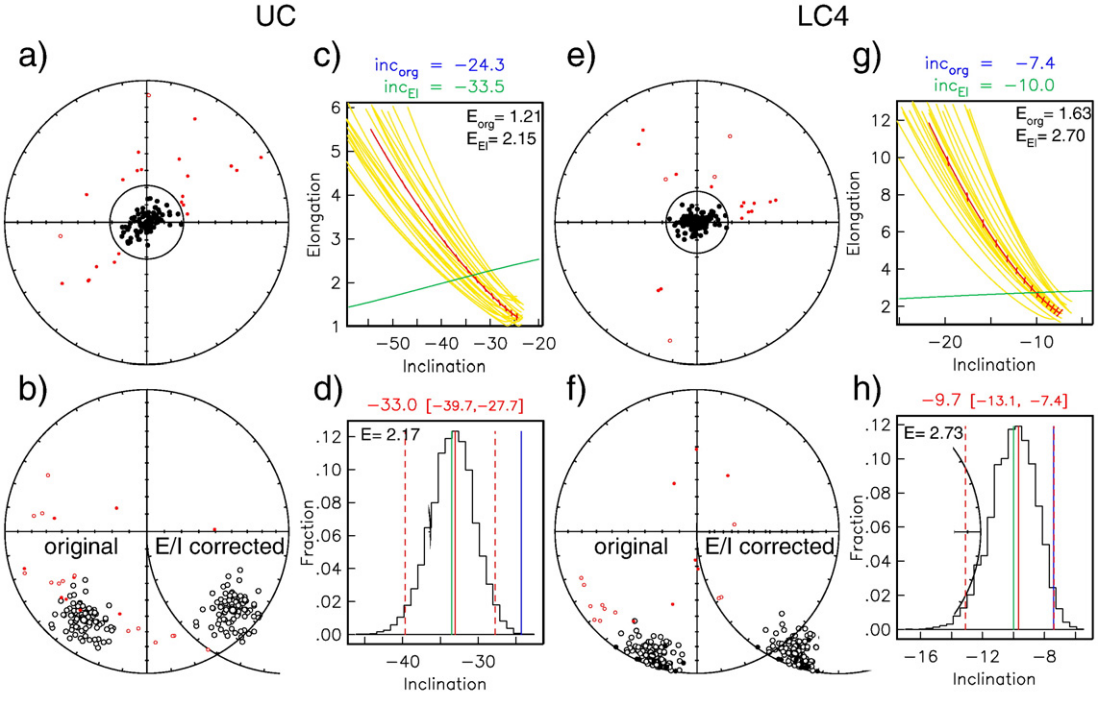


**Fig. 8.** Equal area projections of the individual VGP directions before *E/I* correction (a and e) and equal area projections of the individual ChRM directions before (b and f, left side) and after (b and f, right side) *E/I* correction (symbols as in Fig. 7) (Tauxe and Kent, 2004) with corresponding elongation vs. inclination (c and g) and fraction (of 5000 bootstraps) vs. inclination plots (d and h) for UC (a–d) and LC4 (e–h). In the elongation vs. inclination plots the *E/I* for the TK03.GAD model (green dashed line) and for the datasets (red barbed line) for different degrees of flattening are plotted. The red barbs indicate the direction of elongation (horizontal is E–W and vertical is N–S). Also shown are examples (yellow lines) from 20 (out of 5000) bootstrapped data sets. The crossing points (if the dataset intersects the model) represent the inclination/elongation pair most consistent with the TK03.GAD model, given as $inc_{EI}$ and $E_{EI}$ (in green) above the panel; $inc_{org}$ = original inclination, $E_{org}$ = original elongation of the dataset. In the fraction/inclination plot, a histogram of crossing points from 5000 bootstrapped data sets is shown. The most frequent inclination (solid red vertical line; dashed red vertical lines denote the 95% bootstrap errors) is given as value (and error range) on top of the panel; the inclinations of the original distribution (blue vertical line) or the intersection with the model (green vertical line) are indicated; $E$ = the elongation resulting from the bootstrapped data sets.

from 10 to 200 μA/m, with some exceptions that have initial intensities up to 15,000 μA/m. Curie temperatures for the limestone samples are 570 °C–580 °C (Fig. 5e), so the magnetic carrier in the samples is magnetite. Thermal and AF demagnetisation yield identical results.

Initial intensities of the claystones (MC2) range 200–5000 μA/m. Thermomagnetic treatment shows a mainly paramagnetic decay (Fig. 5f), but a drop in intensity around 300 °C suggests either an iron sulfide as main carrier, or points to an inversion of maghemite.

The medium temperature/medium coercivity component in specimens from site MC1 was interpreted as the ChRM direction (Figs. 6c and 7j). Thermal demagnetisation of the claystone specimens of MC2 gave three components: a low temperature (~20 °C–270 °C) direction (Fig. 7c), a high temperature (>400 °C) and high coercive force component (>100 mT) direction that yields the present-day geocentric axial dipole (GAD) direction (Fig. 7a), and a medium temperature component (~300 °C–400 °C) that yields directions similar to those obtained in the AF demagnetised claystone and limestone samples (Figs. 6c, 7j and 9e–f). Because this medium temperature component was largely overprinted by the high temperature component (Fig. 7c), these results could not be used for further analysis.

AF demagnetisation diagrams of the claystones of MC2 yield three components: a low coercive force component (~0–20 mT) (Fig. 7a), a medium coercive force component (~20–60 mT) (Fig. 7j) and a high coercive force component (>60 mT) (Fig. 7c), that in general do not trend towards the origin, with some exceptions of the middle coercive force component. This medium coercive force component is similar to the directions in the other Carboniferous sites, although in a part of the samples it is heavily affected by a high coercive force component (>60 mT) (Fig. 9c). To discriminate between samples that were heavily affected by this high coercive force component and samples that could be used for determining ChRM directions, decay curves of the specimens were plotted and compared (Fig. 9b, d and g). In Fig. 9g, a clear difference between the samples that were significantly affected by the high coercive force component and samples that still yield a Carboniferous direction is clearly visible. The former were rejected from further analysis.

The mean directions of the limestones (MC1) and claystones (MC2) have a common true mean direction (ctmd) ($\gamma = 4.0 < \gamma_c = 5.6$, classification B). The mean ChRM direction for MC1 and MC2 (corrected for tilt, $N = 84$) is: $D = 223.4$ and $I = -15.0$ (Table 1, Fig. 7j). Correction for inclination error would possibly give rather different results for limestones and claystones. Therefore we applied the *E*/*I* method to sites MC1 and MC2 separately, before applying the method to the combined data sets in order to check for differences in correction. We must take into account that the number of individual directions per data set is possibly too low to apply the *E*/*I* method, but corrections for both data sets separately are very similar (Table 1). Therefore, we decided to combine both data sets for *E*/*I* correction, resulting in a significantly steeper inclination of $I = -22.4$.

### 3.3.5. Kasimovian/Gzelian

Site UC was drilled in upper Carboniferous limestones (upper Kasimovian or lower Gzelian, marker limestone O-6-1 of Popov (1965)). The marker limestone was sampled at two locations (several tens of meters apart), each in ~2 m of stratigraphy, covering the entire thickness of the limestone bed (see Table 1). The total number of demagnetised specimens is 114, out of which 18 specimens were demagnetised thermally (Fig. 6b). The remaining specimens were demagnetised using AF treatment, after thermal treatment until 250 °C or 300 °C. Initial intensities range from ~100 to 600 μA/m. We found a Curie temperature of 570 °C (Fig. 5d), indicating that the magnetic carrier is magnetite. An additional inflection point between ~300 and 350 °C could indicate an inversion of some maghemite. The ChRM direction that was corrected for bedding tilt ($N = 86$) is: $D = 215.5$ and $I = -24.3$ (Table 1, Fig. 7i). Correction for inclination error yields $I = -33.0$, which is statistically significant (Fig. 8, Table 1).

### 3.3.6. Asselian

Sites LP1, LP2 and LP3 were drilled in lower Permian (Asselian) red beds, only several tens of meters apart. The red beds in site LP3 are coarser than the red beds of sites LP1 and LP2. Each of the three sites was sampled within ~2 stratigraphic meters: the total stratigraphic thickness of the sites together is ~6 m. The total number of thermally demagnetised specimens is 208. Initial intensities range from ~3 to 7 mA/m in LP1 and LP2, and from ~7 to 10 mA/m in LP3). Néel temperatures of 660°–675 °C (Fig. 5a–c), and additional inflections in the thermomagnetic curves of LP1 and LP3 (Fig. 5a and c) representing Curie temperatures of 580 °C suggest that both hematite and magnetite are the magnetic carriers. We interpreted the magnetite component as the ChRM direction (Fig. 6a).

Since LP1, LP2 and LP3 were sampled from similar lithologies and within the same formation, and only several tens of meters apart, similar ChRM directions were expected. However, LP3 yields a direction very different from LP1 and LP2 (Table 1). Because the mean direction of LP3 plots on a great circle between the mean directions of LP1 and LP2 and the GAD field in the Donbas area (Fig. 7e–h), we interpret this as a remagnetisation that is transitional direction between the primary, early Permian direction and the GAD field. This is likely related to the slightly coarser nature of the LP3 sediments, and we therefore exclude LP3 from further analysis. The ChRM directions of LP1 and LP2 do not pass a ctmd test (McFadden and Lowes, 1981). From Fig. 7h, it can be seen that LP1 was also partly influenced by a later overprint. Only LP2 is used for further analysis.

Out of the 50 specimens from LP2 that were used for final calculation of the ChRM, 10 specimens have a ChRM direction derived from great-circle analysis (McFadden and McElhinny, 1988). The mean ChRM direction (bedding tilt corrected) is $D = 212.0$ and $I = -29.5$ (Table 1, Fig 7f). If directions using great-circle analysis are excluded from analysis, the resulting ChRM is identical the same within error: $D = 211.0$ and $I = -29.0$. Correction for inclination error was not applied, since the number of specimens does not approach the minimum required number ($N > 100$).

## 4. Discussion

The ChRM directions from the lower Carboniferous to lower Permian limestones, claystones and red beds presented here are very consistent within each site (Fig. 7), they differ significantly per site, and all sites recorded reversed polarities. A fold test could not be applied to our datasets since we sampled the different time intervals at a single location, with only a small variation in bedding tilt. Iosifidi and Khramov (2002) did apply a fold test with a positive result to their lower Permian samples from the Donbas basin, which were collected from the same formation as our lower Permian samples.

The reversed polarity of the ChRM directions is in line with the age of MC, UC and LP, which were sampled within rocks that were deposited during the Permo-Carboniferous Reversed Superchron (PCRS), which lasted from ~317 to ~265 Ma (Opdyke et al., 2000; Menning et al., 2006). During the Carboniferous period preceding the PCRS, several normal polarity chrons are known (Davydov et al., 2004). Although the Carboniferous polarity time scale is not well-determined, the normal polarity chrons reported by Davydov et al. (2004) in the time scale of Gradstein et al. (2004) cover only ~31% of the period preceding the PCRS. This implies that in the age range of our sites the probability is 70% that we sampled reversed polarity intervals. A Permian thermal event, recognised in fission track analysis and vitrinite-reflectance studies (Sachsenhofer et al., 2002; Spiegel et al., 2004), possibly related to a magmatic episode in the Donbas Foldbelt during the early Permian (Alexandre et al., 2004), could have caused a partial reversed polarity remagnetisation of the magnetic signal. However, the low inclinations we find here show a trend toward steeper inclinations with time, which is inconsistent with a remagnetisation event influencing our sites (Fig. 3). Indeed, several

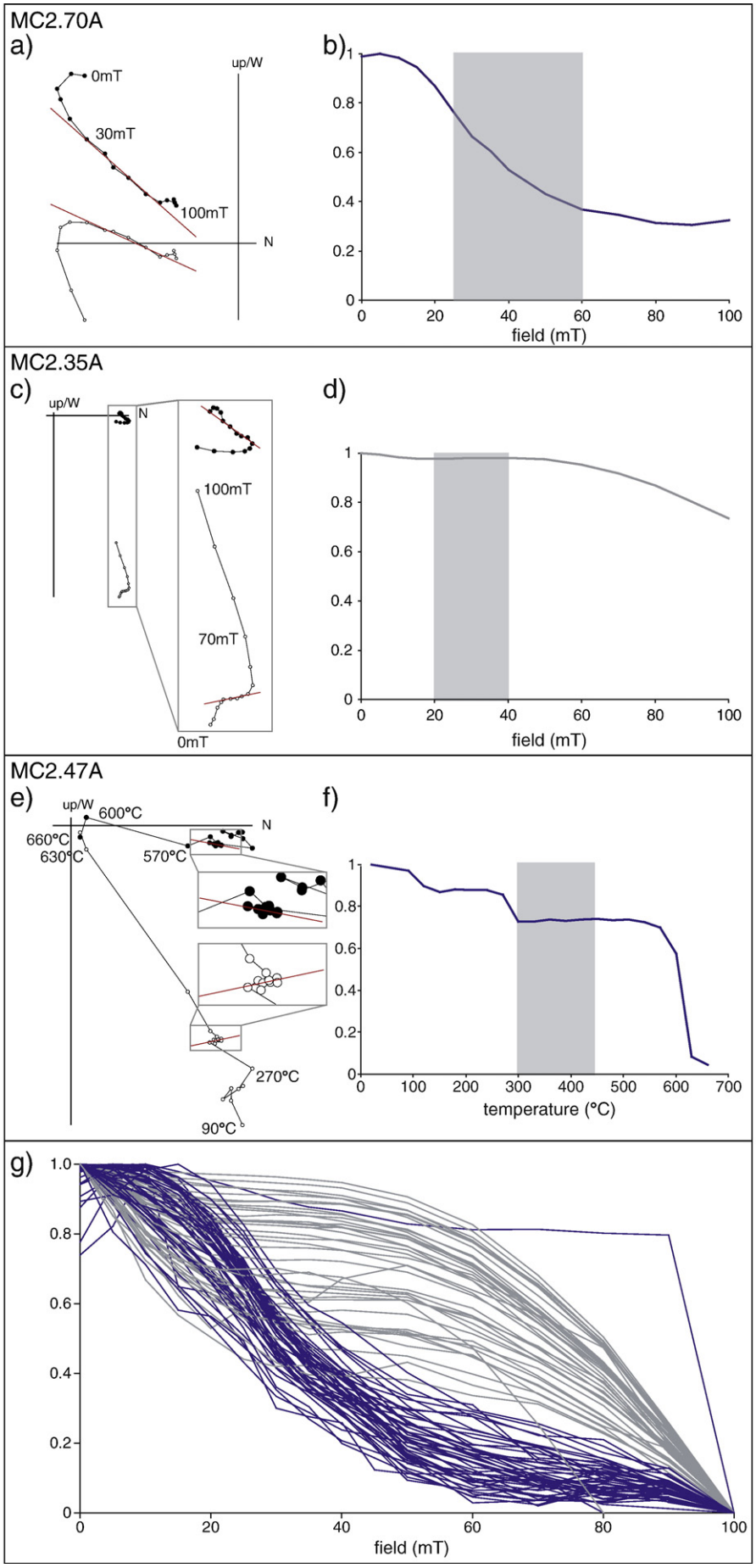
MC2.70A
a)
up/W
0mT
30mT
100mT
N
b)
1
0.8
0.6
0.4
0.2
0
0
20
40
60
80
100
field (mT)
MC2.35A
c)
up/W
N
100mT
70mT
0mT
d)
1
0.8
0.6
0.4
0.2
0
0
20
40
60
80
100
field (mT)
MC2.47A
e)
up/W
600°C
N
660°C
630°C
570°C
270°C
90°C
f)
1
0.8
0.6
0.4
0.2
0
0
100
200
300
400
500
600
700
temperature (°C)
g)
1.0
0.8
0.6
0.4
0.2
0
0
20
40
60
80
100
field (mT)

sites, recorded a present-day or recent GAD field direction (Fig. 7a–d), but it is clearly distinct from the component that we interpret as a ChRM. The statistically significant directional difference between the sites of different age intervals also implies that the ChRM in all sites older than Permian cannot represent a Permian remagnetisation. We therefore believe that our ChRM directions represent an original magnetisation acquired at the time the rocks were formed.

The *E*/*I* method gives a significant change in inclination for sites LC1_2, MC and UC. This is an indication that the NRM was acquired before compaction. Correction with the *E*/*I* model for sites LC3 and LC4 produces a small but not significant change. There are several possible explanations for this. It may imply that NRM acquisition was slightly delayed, and acquired after early dewatering and compaction of the sediments, possibly during early diagenesis (e.g. Van Hoof and Langereis (1991)). A more likely explanation is that, because the sediments of sites LC3 and LC4 were deposited nearest to the equator, inclination shallowing is not significant, because of the low magnetic field inclination.

Therefore, we conclude that the observed inclination/paleolatitude and declination trends of the sampled time interval (Table 1, Fig. 3) are the result of plate tectonics and/or local tectonic rotations. We must now consider whether the Donbas region formed part of stable Europe, so that corresponding paleopoles can be used for the APW path for this time interval.

The only AMS results that did not give random directions are from sites LP and MC2. Those results (Fig. 4) either reflect NNW–SSE compression or the direction of currents during deposition of the sediments. A paleocurrent direction is generally only recorded in coarser grained sediments and high-energy sedimentary environments, which could be the case for the red beds of site LP. Paleoflow directions are however absent for this region, and therefore we can only speculate that the AMS orientation of both sites is a reflection of NNW–SSE compression. This is in very good agreement with paleostress data from Saintot et al. (2003a), that indicate an Eo-Alpine strike–slip regime with NNW–SSE trending $\sigma_1$.

Outside Scandinavia, there are no Carbonifeous and early Permian datasets from Baltica that are incorporated into the APW paths (Torsvik and Cocks, 2005; Torsvik et al., 2008a). To discuss our data in the large-scale framework of global plate movements, the $A_{95}$ error envelope of the APW paths of Torsvik et al. (2008a) (310–0 Ma) and Torsvik and Cocks (2005) (360–310 Ma) is plotted in Fig. 3, recalculated to the city of Donets (48°N, 37.8°E). The APW path of Laurussia at 350 and 360 Ma (Torsvik and Cocks, 2005) however, is constructed on the basis of a single pole entry and is therefore very poorly constrained.

Our datasets without correction for inclination shallowing with the *E*/*I* model (Tauxe and Kent, 2004) show that in general, the paleolatitudes agree very well with those of the Eurasian polepaths (Fig. 1), although our oldest pole (LC4) and our two youngest poles (UC and LP2) yield slightly higher paleolatitudes. Applying the *E*/*I* correction slightly increases the paleolatitudes (Fig. 1). In published APW paths, the paleolatitude may be underestimated because of unrecognised or uncorrected inclination shallowing in sediments (Torsvik and Cocks, 2005; Torsvik et al., 2008a), although the majority of the data points used to construct the APW path between 360 Ma and 290 Ma is based on volcanic rocks (25 out of 38 entries).

Our data from the lower Permian red beds (LP2), yield nearly-identical results to data from time-equivalent red beds in the Donbas Foldbelt studied by Iosifidi and Khramov (2002) and Iosifidi et al. (2010) (Fig. 3, green stars). Their positive fold tests on the data from lower Permian and upper Carboniferous rocks (McFadden and Jones, 1981; Watson and Enkin, 1993), confirm our confidence in the primary origin of the directions obtained from our sites. The lower Permian results of Iosifidi et al. (2010) supersede those of Iosifidi and Khramov (2002), since they are from the same formation, but with more samples; the difference is negligible. Their upper Carboniferous data are new. Iosifidi et al. (2010) isolated a component mainly residing in pigmentary hematite in the red beds, yielding a higher inclination than the component residing in detrital, specular hematite. Since pigmentary hematite is formed after deposition, they argue that these components have no significant inclination error. This was also observed in redeposition experiments of the Kartamysh Formation, performed by Khramov et al. (1987).

Comparing the declinations of our three youngest sites (MC, UC and LP2) with the published APW paths (Fig. 3), they plot reasonably well within the error. The oldest, southern three sites (LC4, LC3 and LC1_2), have a consistently different declination both compared to the APW paths and to the youngest, northern three sites, suggesting a rotation of ~20°. This rotation difference could imply that in the time span between deposition of the sediments of sites LC1_2 and MC (~8 Ma), the region rotated ~20°, which is not recognised in the APW path (Torsvik and Cocks, 2005). Here, we must again take into account however, that no Baltica poles outside Scandinavia are incorporated in the Carboniferous APW path. Another way to explain the rotation difference between the youngest sites and oldest sites is by introducing a local rotation effect between the northern and central part of the Donbas Foldbelt and its southern part, which has a diverging strike from the general trend in the region. This strike difference corresponds both in sense and magnitude to the declination deviation of our oldest sites from the published APW paths. Anomalous N–S trending thrusts and folds in the sampling area of LC4 and LC3 were recognised by Saintot et al. (2003b), which they ascribed to the Cimmerian (late Triassic to Jurassic) and Alpine (Cretaceous/Tertiary boundary) reactivation of shallow inherited structures at the southern margin of the basin. Numerical models in their study that calculate stress axis trends, predict a counterclockwise rotation of ~15° with respect to the surrounding area for the area between the Yujni and Vassiliev Faults (Fig. 2b). This is in good agreement with our relative paleomagnetic rotations of sites LC4 and LC3. Site LC1_2 was sampled in the vicinity of a N–S trending thrust fault, which could have possibly caused a similar effect. We therefore suggest that the deviation is likely the result of local CCW vertical-axis rotations in the southern part, implying that we cannot use the directions of these sites for determining pole positions for further analysis of the APW path. The sites are also situated in the region where Arthaud and Matte (1977) proposed the shear zone that accommodated Pangea transformation. The shear zone however, would cause clockwise rotations, which is opposite to the counterclockwise (CCW) rotations of our oldest three sites.

In Fig. 1b–c, we compare a continent reconstruction at 300 Ma based on our data from LP2, with those of Torsvik et al. (2008a) and Van der Voo and Torsvik (2004) at 300 Ma. Laurussia is displayed in grey, according to the pole from site LP2. Because Laurentia and Eurasia were part of the same tectonic plate (called Laurussia) in Pangean times, usage of Laurentian poles is allowed for Laurentia. Comparing our data to the Gondwana reconstructions, there is no overlap between the northern and southern continents. The same holds for a reconstruction using the latest Carboniferous pole UC (not displayed here). Therefore, these two datasets, would not require a Pangea B type reconstruction. As mentioned above, Van der Voo and Torsvik (2004) partly solve the overlap problem in the early Permian

**Fig. 9.** a), c) and e) Demagnetisation diagrams of characteristic samples of the claystones of site MC. b), d) and f) NRM intensity upon AF demagnetisation normalised by initial NRM intensity. Grey rectangle indicates AF/temperature steps that were used for calculation of the ChRM directions. g) NRM intensity upon AF demagnetisation normalised by initial NRM intensity of all individual samples of site MC2 normalised (total intensity). Highest AF/temperature step intensity was set to zero for display purposes. Grey (light-coloured) curves indicate the curves of the samples that were rejected and blue (dark-coloured) curves indicate the samples that were used for calculation of the mean ChRM direction of site MC. The ChRM directions belonging to the grey (light-coloured) curves were typically affected by a later acquired NRM component.

by considering only the highest quality European poles. They selected these on the basis of paleomagnetic quality, age control and also rock type (volcanics) to avoid the possibility of inclination shallowing in sediments (Van der Voo, 1990). In this way, Eurasia is located almost 10° further north at 280 Ma. If we compare our Permian data to Van der Voo and Torsvik's (2004) presented polepath at 300 Ma, our data plot even ~5° further to the north (Fig. 1b). Moreover, our Carboniferous data points (Fig. 3) show a very general and gentle northward motion of Laurussia (at Donets) from near-equatorial position (3–5°N) to ~18°N, which strengthens the interpretation of a more northerly position of Laurussia during Pangean times, in line with Van der Voo and Torsvik (2004). Because of the juxtaposition of Laurentia and Eurasia, this means that, in the early Permian, our data from the Donbas Foldbelt would place Laurussia at a more northerly position, explaining the Pangea misfit without a need to introduce an octupole contribution to the Earth's magnetic field (e.g. Torsvik and Cocks, 2004).

Recently, Kodama (2009) and Bilardello and Kodama (2010) reassessed ages and corrected Carboniferous poles from the present-day eastern part of North America that likely occupied a position just south of the equator in the Pangea configuration for inclination error, using the inclination-shallowing correction method developed by Tan and Kodama (2003). The effect of an inclination correction for Laurentian paleolatitudes is of course inverse: following their data, Laurussia was positioned more southward rather than our more northward latitudes obtained from Ukraine. We illustrated this effect for the Donbas region in Fig. 3 (purple arrows) for the corrected results from the Glenshaw, Shepody and Maringouin Formations. More southerly positions of southwestern Laurussia would significantly increase the overlap of Gondwana and Laurussia, clearly requiring a Pangea B configuration. However, combining their results with ours would not only imply the necessity for a major shear zone to come from a Pangea B to a Pangea A configuration in the Triassic (Fig. 1), but also implies major stretching and subsequent shortening of Laurentia. This would make the Pangea controversy quite different than known so far. More important, the Carboniferous poles from Gondwana are largely based on poles from sediments (Torsvik and Van der Voo, 2002), that were are not corrected for inclination shallowing. Our data, the data from Bilardello and Kodama (2010) and Kodama (2009) show that correction for inclination shallowing affects the position of the continents. Therefore, application of a method to correct for shallowing would result in a more southerly position of Gondwana, (partly) removing the overlap between the northern and southern continents. The strongly contrasting results of our study and those of Bilardello and Kodama (2010) and Kodama (2009) show that the Carboniferous paleomagnetic data still contain enough grounds for a Pangea controversy. Furthermore, data should cover and be representative for an entire continent, which is not the case for the Carboniferous and early Permian Eurasian polepaths, since no reliable eastern European and Asian data entries are available. In the late Permian pole path, many poles from southern France have been included, mainly from sediments (red beds). It was recently pointed out by Bazhenov and Shatsillo (2010) that at least during the late Permian, the French group of poles shows a significant deviation with respect to the late Permian poles of the remaining part of the continent. The authors suggest that this is caused by a hitherto unrecognised rotation of southern France. A similar effect of Carboniferous and early Permian groups of poles on the Eurasian polepath, would obviously have large implications for Pangea reconstructions. Paleomagnetic data were at the basis of the Pangea controversy, and although more and better data became available, the controversy remains.

## 5. Conclusions

Summarising, we present new Eurasian Carboniferous and early Permian sedimentary paleomagnetic datasets from sediments, and the only ones that are large enough to enable *E*/*I* correction for inclination shallowing in sediments (Tauxe and Kent, 2004), thereby improving the quality of these paleopoles. This allows us to constrain the Permo-Carboniferous paleolatitude of Laurussia at the position of the Donbas Foldbelt.

In general, our results yield similar or higher values for paleolatitude than those previously used to construct the APW path. Unfortunately, our lower and middle Carboniferous poles are most likely affected by a tectonic rotation, and therefore can only indicate reliable paleolatitudes.

Our upper Carboniferous and lower Permian data do not require a Pangea B type reconstruction. The paleolatitudes of Laurussia calculated from our poles enable a Pangea A reconstruction, and do not require an overlap of northern and southern Pangea terranes. However, a recent correction and reassessment of North American (Laurentian) paleomagnetic data from recent studies suggest quite the opposite and even require changes in the dimensions of Laurussia through time. Therefore, the Pangea A vs. B controversy is as lively as during the past 30+ yr, since Irving (1977).

## Acknowledgements

The authors would like to thank Hemmo Abels, Flora Boekhout, Wolter Bosch and Constantin Pechnikov for their field assistance. We thank Shell International Exploration and Production, Rijswijk, the Netherlands, and Shell Ukraine, for logistical and financial support; Calum MacDonald, Mark Geluk and Maxim Vityk, as well as Sergiy Stovba from NAUKA Ukraine are thanked for discussion. For the use of the data of their study, we would like to acknowledge A.G. Iosifidi, C. Mac Niocaill, A.N. Khramov, M.J. Dekkers and V.V. Popov. We would like to thank two anonymous reviewers for their constructive comments. An earlier version of this manuscript benefited from the comments of Sacha Iosifidi and three anonymous reviewers. M.J.M.M. acknowledges the Netherlands Research Centre for Integrated Solid Earth Sciences (ISES) and the Netherlands Organization for Scientific Research (NWO) for financial support.

## Appendix A. Supplementary data

Supplementary data associated with this article can be found, in the online version, at doi:10.1016/j.epsl.2010.05.028.

## References

Alexandre, P., Chalot-Prat, F., Saintot, A., Wijbrans, J., Stephenson, R., Wilson, M., Kitchka, A., Stovba, S., 2004. The 40Ar/39Ar dating of magmatic activity in the Donbas Fold Belt and the Scythian Platfrom (East European Craton). Tectonics 23 (TC5002). doi:10.1029/2003TC001582.

Angiolini, L., Gaetani, M., Muttoni, G., Stephenson, M.H., Zanchi, A., 2007. Tethyan oceanic currents and climate gradients 300 m.y. ago. Geology 35 (12), 1071–1074. doi:10.1130/G24031A.1.

Arthaud, F., Matte, P., 1977. Late Paleozoic strike–slip faulting in southern Europe andnorthern Africa: result of a right-lateral shear zone between the Appalachians and the Urals. Geol. Soc. Am. Bull. 88, 1305–1320.

Bazhenov, M., Shatsillo, M., 2010. Late Permian palaeomagnetism of Northern Eurasia: data evaluation and a single-plate test of the geocentric axial dipole model. Geophys. J. Int. 180, 136–146. doi:10.1111/j.1365-246X.2009.04379.x.

Besse, J., Courtillot, V., 2002. Apparent and true polar wander and the geometry of the geomagnetic field in the last 200 million years. J. Geophys. Res. 107 (B11). doi:10.1029/2000JB000050.

Bilardello, D., Kodama, K.P., 2010. Palaeomagnetism and magnetic anisotropy of Carboniferous red beds from the Maritime Provinces of Canada: evidence for shallow palaeomagnetic inclinations and implications for North American apparent polar wander. Geophys. J. Int. 180 (3), 1013–1029. doi:10.1111/j.1365-246X.2009.04457.x.

Butler, R.F., 1992. Paleomagnetism: Magnetic domains to geologic terranes. Blackwell Scientific Publications, Boston, 238 pp.

Chekunov, A.V., Kaluzhnaya, L.T., Ryabchun, L.I., 1993. The Dniepr–Donets paleorift, Ukraine, deep structures and hydrocarbon accumulations. J. Petrol. Geol. 16, 183–196.

Creer, K.M., Irving, E., Runcorn, S.K., 1954. The direction of the geomagnetic field in remote epochs in Great Britain. J. Geomagn. Geoelectr. 6, 163–168.

Davydov, V., Wardlaw, B.R., Gradstein, F.M., 2004. The Carboniferous period. In: Gradstein, F.M., Ogg, J.G., Smith, A.G. (Eds.), A Geologic Time Scale 2004. Cambridge University Press, pp. 222–237.

Davydov, V.I., Crowley, J.L., Schmitz, M.D., Poletaev, V.I., 2010. High-precision U–Pb zircon age calibration of the global Carboniferous time scale and Milankovitch-

band cyclicity in the Donets Basin, eastern Ukraine. Geochem. Geophys. Geosyst. 11 (Q0AA04). doi:10.1029/2009GC002736.
Dietz, R.S., 1961. Continent and ocean basin evolution by spreading of the sea floor. Nature 190, 854–857.
Du Toit, A.L., 1937. Our Wandering Continents. Edinburgh, Oliver and Boyd.
Fisher, D.A., 1953. Dispersion on a sphere. Proceedings of the Royal Society of London A 217, 295–305.
Gong, Z., Dekkers, M.J., Dinarès-Turell, J., Mullender, T.A.T., 2008a. Remagnetization mechanism of Lower Cretaceous rocks from the Organyà Basin (Pyrenees, Spain). Stud. Geophys. Geod. 52, 187–210.
Gong, Z., Langereis, C.G., Mullender, T.A.T., 2008b. The rotation of Iberia during the Aptian and the opening of the Bay of Biscay. Earth Planet. Sci. Lett. 273 (1–2), 80–93.
Gradstein, F.M., Ogg, J.G., Smith, A.G., Agterberg, F.P., Bleeker, W., Cooper, R.A., Davydov, V., Gibbard, P., Hinnov, L.A., House, M.R., Lourens, L., Luterbacher, H.P., McArthur, J., Melchin, M.J., Robb, L.J., Shergold, J., Villeneuve, M., Wardlaw, B.R., Ali, J., Brinkhuis, H., Hilgen, F.J., Hooker, J., Howarth, R.J., Knoll, A.H., Laskar, J., Monechi, S., Plumb, K.A., Powell, J., Raffi, I., Röhl, U., Sadler, P., Sanfilippo, A., Schmitz, B., Shackleton, N.J., Shields, G.A., Strauss, H., Van Dam, J., van Kolfschoten, T., Veizer, J., Wilson, D., 2004. A New Geologic Time Scale, with Special Reference to Precambrian and Neogene. Cambridge University Press.
Gutierrez-Alonso, G., Fernandez-Suarez, J., Weil, A.B., Murphy, J.B., Nance, R.D., Corfu, F., Johnston, S.T., 2008. Self-subduction of the Pangaean global plate. Nat. Geosci. 1, 549–553.
Heezen, B.C., 1960. The rift in the ocean floor. Sci. Am. 203, 98–110.
Hrouda, F., 1982. Magnetic anisotropy of rocks and its application in geology and geophysics. Surv. Geophys. 5, 37–82.
Iosifidi, A.G., Khramov, A.N., 2002. Paleomagnetism of Upper Carboniferous and Lower Permian deposits of the East European Platform: a key paleomagnetic pole and kinematics of collision with the Urals. Izvestiya-Phys. Solid Earth 38 (5), 389–403.
Iosifidi, A.G., Mac Niocaill, C., Khramov, A.N., Dekkers, M.J., Popov, V.V., 2010. Palaeogeographic implications of differential inclination shallowing in permo-carboniferous sediments from the donets basin, Ukraine. Tectonophysics 490, 229–240.
Irving, E., 1977. Drift of the major continental blocks since the Devonian. Nature 270, 304–309.
Jelinek, V., 1981. Characterization of the magnetic fabric of rocks. Tectonophysics 79 (3–4), T63–T67.
Jelinek, V., 1984. On a mixed quadratic invariant of the magnetic-susceptibility tensor. J. Geophys. Z. Geophys. 56 (1), 58–60.
Kent, D.V., Smethurst, M.A., 1998. Shallow bias of paleomagnetic inclinations in the Paleozoic and Precambrian. Earth Planet. Sci. Lett. 160, 391–402.
Khramov, A.N., Goncharev, G.I., Komissarova, R.A., Pisarevsky, S.A., Pogarskaya, I.A., 1987. Paleomagnetology. Springer-Verlag, Berlin.
Kirschvink, J.L., 1980. The least-square line and plane and the analysis of paleomagnetic data. Geophys. J. R. Astron. Soc. 62, 699–718.
Kodama, K.P., 2009. Simplification of the anisotropy-based inclination correction technique for magnetite- and haematite-bearing rocks: a case study for the Carboniferous Glenshaw and Mauch Chunk Formations, North America. Geophys. J. Int. 176 (2), 467–477. doi:10.1111/j.1365-246X.2008.04013.x.
Köppen, W., Wegener, A., 1924. Die Klimate der geologischen Vorzeit. Bornträge, Berlin.
McFadden, P.L., Jones, D.L., 1981. The fold test in palaeomagnetism. Geophys. J. R. Astron. Soc. 6, 53–58.
McFadden, P.L., Lowes, F.J., 1981. The discrimination of mean directions drawn from Fisher distributions. Geophys. J. R. Astrol. Soc. 67, 19–33.
McFadden, P.L., McElhinny, L.W., 1988. The combined analysis of remagnetization circles and direct observations in palaeomagnetism. Earth Planet. Sci. Lett. 87, 161–172.
McFadden, P.L., McElhinny, M.W., 1990. Classification of the reversal test in palaeomagnetism. Geophys. J. Int. 103, 725–729.
Menning, M., Alekseev, A.S., Chuvashov, B.I., Davydov, V.I., Devuyst, F.-X., Forke, H.C., Grunt, T.A., Hance, L., Heckel, P.H., Izokh, N.G., Jin, Y.-G., Jones, P.J., Kotlyar, G.V., Kozur, H.W., Nemyrovska, T.I., Schneider, J.W., Wang, X.-D., Weddige, K., Weyer, D., Work, D.M., 2006. Global time scale and regional stratigraphic reference scales of Central and West Europe, East Europe, Tethys, South China, and North America as used in the Devonian–Carboniferous–Permian Correlation Chart 2003 (DCP 2003). Palaeogeogr. Palaeoclimatol. Palaeoecol. 240, 318–372.
Morel, P., Irving, E., 1981. Paleomagnetism and the Evolution of Pangea. J. Geophys. Res. 86 (B3), 1858–1872.
Mullender, T.A.T., van Velzen, A.J., Dekkers, M.J., 1993. Continuous drift correction and separate identification of ferromagnetic and paramagnetic contributions in thermomagnetic runs. Geophys. J. Int. 114, 663–672.
Müller, R.D., Royer, J.-Y., Lawver, L.A., 1993. Revised plate motions relative to the hotspots from combined Atlantic and Indian Ocean hotspot tracks. Geology 21 (3), 275–278.
Muttoni, G., Kent, D.V., Channell, J.E.T., 1996. Evolution of Pangea: paleomagnetic constraints from the southern Alps, Italy. Earth Planet. Sci. Lett. 140, 97–112.
Muttoni, G., Kent, D.V., Garzanti, E., Brack, P., Abrahamsen, N., Gaetani, M., 2003. Early Permian Pangea 'B' to Late Permian Pangea 'A'. Earth Planet. Sci. Lett. 215, 379–394.
Muttoni, G., Gaetani, M., Kent, D.V., Sciunnach, D., Angiolini, L., Berra, F., Garzanti, E., Mattei, M., Zanchi, A., 2009. Opening of the Neo-Tethys Ocean and the Pangea B to Pangea A transformation during the Permian. GeoArabia 14 (4), 17–48.
Norton, I.O., 2000. Global hotspot reference frames in plate motion. In: Richards, M.A., Gordon, R.G., van der Hilst, R.D. (Eds.), The History and Dynamics of Global Plate Motion, pp. 339–357.
Ogg, J.G., Ogg, G., Gradstein, F.M., 2008. The Concise Geologic Time Scale. Cambridge University Press, Cambridge.
Opdyke, N.D., Roberts, J., Claoue-Long, J., Irving, E., Jones, P.J., 2000. Base of the Kiaman: its definition and global stratigraphic significance. GSA Bull. 112 (9), 1315–1341.
Popov, V.S., 1965. The geological map of pre-Mesozoic sediments of the Ukrainian part of the Great Donbas, Ministry of Geology of USSR.
Richards, M.A., Duncan, R.A., Courtillot, V.E., 1989. Flood basalts and hotspot tracks: plume heads and tails. Science 246, 103–107.
Rochette, P., Vandamme, D., 2001. Pangea B: an artifact of incorrect paleomagnetic assumptions? Ann. Geofis. 44 (3), 649–658.
Sachsenhofer, R.F., Privalov, V.A., Zhykalyak, M.V., Bueker, C., Panova, E.A., Rainer, T., Shymanovskyy, V.A., Stephenson, R., 2002. The Donets Basin (Ukraine/Russia): coalification and thermal history. Int. J. Coal Geol. 49, 33–55.
Saintot, A., Stephenson, R., Brem, A., Stovba, S., Privalov, V., 2003a. Paleostress field reconstruction and revised tectonic history of the Donbas fold and thrust belt (Ukraine and Russia). Tectonics 22 (5), 1059.
Saintot, A., Stephenson, R., Stovba, S., Maystrenko, Y., 2003b. Structures associated with inversion of the Donbas Foldbelt (Ukraine and Russia). Tectonophysics 373, 181–207.
Schaltegger, U., Brack, P., 2007. Crustal-scale magmatic systems during intracontinental strike–slip tectonics: U, Pb and Hf isotopic constraints from Permian magmatic rocks of the Southern Alps. Int. J. Earth Sci. 96, 1131–1151. doi:10.1007/s00531-006-0165-8.
Spiegel, C., Sachsenhofer, R.F., Privalov, V.A., Zhykalyak, M.V., Panova, E.A., 2004. Thermotectonic evolution of the Ukrainian Donbas Foldbelt: evidence from zircon and apatite fission track data. Tectonophysics 383, 193–215.
Stephenson, R.A., Yegorova, T., Brunet, M.-F., Stovba, S., Wilson, M., Starostenko, V., Saintot, A., Kusznir, N., 2006. Late Palaeozoic intra-cratonic basins on the East European Craton and its margins. In: Gee, D.G., Stephenson, R.A. (Eds.), European Lithosphere Dynamics, London: The Geological Society of London, 32, pp. 463–479.
Stovba, S.M., Stephenson, R.A., 1999. The Donbas Foldbelt: its relationships with the uninverted Donets segment of the Dniepr–Donets Basin, Ukraine. Tectonophysics 313 (1), 59–83.
Stovba, S.M., Stephenson, R.A., Kivshik, M., 1996. Structural features and evolution of the Dniepr–Donets basin, Ukraine, from regional seismic reflection profiles. Tectonophysics 268, 127–147.
Stovba, S.M., Maystrenko, Y.P., Stephenson, R.A., Kusznir, N.J., 2003. The formation of the south-eastern part of the Dniepr–Donets Basin: 2-D forward and reverse modelling taking into account post-rift redeposition of syn-rift salt. Sed. Geol. 156, 11–33.
Tan, X., Kodama, K.P., 2003. An analytical solution for correcting paleomagnetic inclination error. Geophys. J. Int. 152, 228–236.
Tauxe, L., Kent, D.V., 2004. A simplified statistical model for the geomagnetic field and the detection of shallow bias in paleomagnetic inclinations: was the ancient magnetic field dipolar? In: Channell, J.E.T., Kent, D.V., Lowrie, W., Meert, J.G. (Eds.), Timescales of the Paleomagnetic Field: AGU Geophysical Monograph, 145, pp. 101–115.
Tauxe, L., Kodama, K.P., Kent, D.V., 2008. Testing corrections for paleomagnetic inclination error in sedimentary rocks: a comparative approach. Phys. Earth Planet. Inter. 169, 152–165.
Torcq, F., Besse, J., Vaslet, D., Marcoux, J., Ricou, E., Halawani, M., Basahel, M., 1997. Paleomagnetic results from Saudi Arabia and the Permo-Triassic Pangea configuration. Earth Planet. Sci. Lett. 148, 553–567.
Torsvik, T.H., Cocks, L.R.M., 2004. Earth geography from 400 to 250 Ma: a paleomagnetic, faunal and facies review. J. Geol. Soc. 161, 555–572.
Torsvik, T.H., Cocks, L.R.M., 2005. Norway in space and time: a centennial cavalcade. Norw. J. Geol. 85, 73–86.
Torsvik, T.H., Van der Voo, R., 2002. Refining Gondwana and Pangea palaeogeography: estimates of Phanerozoic non-dipole (octupole) fields. Geophys. J. Int. 151, 771–794.
Torsvik, T.H., Muller, R.D., Van der Voo, R., Steinberger, B., Gaina, C., 2008a. Global plate motion frames: toward a unified model. Rev. Geophys. 46, RG3004. doi:10.1029/2007RG000227.
Torsvik, T.H., Steinberger, B., Cocks, L.R.M., Burke, K., 2008b. Longitude: linking Earth's ancient surface to its deep interior. Earth Planet. Sci. Lett. 276, 273–282.
van der Meer, D.G., Spakman, W., van Hinsbergen, D.J.J., Amaru, M.L., Torsvik, T.H., 2010. Toward absolute plate motions constrained by lower mantle slab remnants. Nat. Geosci. doi:10.1038/ngeo708.
Van der Voo, R., 1990. The reliability of paleomagnetic data. Tectonophysics 184, 1–9.
Van der Voo, R., Torsvik, T.H., 2001. Evidence for late Paleozoic and Mesozoic non-dipole fields provides an explanation for the Pangea reconstruction problems. Earth Planet. Sci. Lett. 187, 71–81.
Van der Voo, R., Torsvik, T.H., 2004. The quality of the European Permo-Triassic paleopoles and its impact on Pangea reconstructions. In: Channell, J.E.T., Kent, D.V., Lowrie, W., Meert, J.G. (Eds.), Timescales of the Internal Geomagnetic Field: AGU Geophysical Monograph, 145, pp. 29–42.
Van Hoof, A.A.M., Langereis, C.G., 1991. Reversal records in marine marls and delayed acquisition of remanent magnetisation. Nature 351, 223–224.
Van Velzen, A.J., Zijderveld, J.D.A., 1995. Effects of weathering on single domain magnetite in early Pliocene marls. Geophys. J. Int. 121, 267–278.
Van Wees, J.D., Stephenson, R.A., Stovba, S.M., Shymanovskyi, V.A., 1996. Tectonic variation in the Dniepr–Donets Basin from automated modelling of backstripped subsidence curves. Tectonophysics 268, 257–280.
Vandamme, D., 1994. A new method to determine paleosecular variation. Phys. Earth Planet. Inter. 85, 131–142.
Watson, G., 1983. Large sample theory of the Langevin distributions. J. Stat. Plann. Infer. 8, 245–256.
Watson, G.S., Enkin, R.J., 1993. The fold test in paleomagnetism as a parameter estimation problem. Geophys. Res. Lett. 20, 2135–2138.
Wegener, A.L., 1915. Die Entstehung der Kontinente und Ozeane.
Zijderveld, J.D.A., 1967. A. C. demagnetization of rocks: analysis of results. In: Collinson, D.W., Creer, K.M., Runcorn, S.K. (Eds.), Methods in Palaeomagnetism. Elsevier, Amsterdam, New York, pp. 254–286.